

When Do Extended Physics-Informed Neural Networks (XPINNs) Improve Generalization?

Zheyuan Hu* Ameya D. Jagtap[†] George Em Karniadakis[†] Kenji Kawaguchi[‡]

Abstract

Physics-informed neural networks (PINNs) have become a popular choice for solving high-dimensional partial differential equations (PDEs) due to their excellent approximation power and generalization ability. Recently, Extended PINNs (XPINNs) based on domain decomposition methods have attracted considerable attention due to their effectiveness in modeling multiscale and multiphysics problems and their parallelization. However, theoretical understanding on their convergence and generalization properties remains unexplored. In this study, we take an initial step towards understanding how and when XPINNs outperform PINNs. Specifically, for general multi-layer PINNs and XPINNs, we first provide a prior generalization bound via the complexity of the target functions in the PDE problem, and a posterior generalization bound via the posterior matrix norms of the networks after optimization. Moreover, based on our bounds, we analyze the conditions under which XPINNs improve generalization. Concretely, our theory shows that the key building block of XPINN, namely the domain decomposition, introduces a tradeoff for generalization. On the one hand, XPINNs decompose the complex PDE solution into several simple parts, which decreases the complexity needed to learn each part and boosts generalization. On the other hand, decomposition leads to less training data being available in each subdomain, and hence such model is typically prone to overfitting and may become less generalizable. Empirically, we choose five PDEs to show when XPINNs perform better than, similar to, or worse than PINNs, hence demonstrating and justifying our new theory.

1 Introduction

Deep learning has revolutionized numerous fields in computer science, such as computer vision and natural language process. Recently, deep neural networks have also been employed to solve partial differential equations (PDEs) and integrated into the field of scientific computing, thanks to their unique optimization [1–4] and generalization [5] abilities. Physics-informed neural networks (PINNs) [6] are among the most popular approaches with a wide variety of successful applications, including heat transfer problems [7], thrombus material properties [8], nano-optics [9], and fluid mechanics [10, 11]. PINNs are used as surrogates of a target solution for solving PDEs, and a solution is found by searching for the best parameters of PINNs that satisfy the physical laws governed by the PDEs. A more recent work [12] proposed Extended PINNs (XPINNs), which improves on PINNs by employing a domain decomposition method for partitioning the PDE problem into several sub-problems on subdomains, where each sub-problem can be solved by individual networks called as sub-PINNs. In XPINNs, the continuity of the PINN functions between each subdomain is maintained. XPINNs facilitate parallel computing, accelerate convergence, and improve generalization empirically. Despite great progress in applications, currently no theoretical understanding exists on when and how XPINNs are better than PINNs.

Recently, some works on theoretical understanding of PINNs have emerged [13–16]. For two-layer networks, Luo and Yang [13] derived prior and posterior generalization bounds for PINNs based on Barron space and Rademacher complexity, whereas Lu et al. [14] provided prior error estimates based on Barron spaces with the softplus activation. For multi-layer networks, Mishra and Molinaro [15] introduced abstract formalism and stability properties of the underlying PDEs to derive generalization bounds, and Shin et al. [16] used the Holder continuity constant to bound the generalization of PINNs. While these previous bounds significantly advanced our theoretical understanding of PINNs, we cannot rely on them to study the advantages and disadvantages of multi-layer XPINNs over PINNs. This is because the previous studies focus on PINNs, and the previous bounds either only apply to two-layer networks or depend on variables that are hard to be computed analytically or numerically. For example, the Holder continuity is often difficult to compute efficiently and the assumption of Holder continuity regularization is not widely adopted in practice. Accordingly, it is necessary to employ different approaches to derive new generalization bounds for the multi-layer XPINN in order to understand its advantages and limitations.

*Department of Computer Science, National University of Singapore, Singapore, 119077 (e0792494@u.nus.edu)

[†]Division of Applied Mathematics, Brown University, Providence, RI 02906, USA (ameya.jagtap@brown.edu, george_karniadakis@brown.edu)

[‡]Center of Mathematical Sciences and Applications, Harvard University, Cambridge, MA 02138, USA (kkawaguchi@fas.harvard.edu)

In this study, we provide an initial step towards understanding how and when XPINNs improve generalization capabilities of PINNs by proving new generalization bounds for multi-layer XPINNs and PINNs. Specifically, we first discuss the Barron space theory for multi-layer networks to define the function space of neural networks. With the regularity assumption on PDE problems, we then derive a prior generalization bound for PINNs with the complexity of a target function measured via its Barron norm. Furthermore, without the regularity assumption on PDE problems, we derive Rademacher complexity bounds of PINNs via capacity controls based on the $(1, \infty)$ norm, which are then used for our posterior generalization bounds for PINNs. We then extend these bounds of PINNs to those of XPINNs by applying the bounds to each of the subdomains in XPINNs and combine them to form the final results. Overall, our theoretical results predict that in terms of generalization, the advantages and disadvantages of XPINNs come from the tradeoff between the reduction in the complexity of decomposed target functions (within each subdomain) and the increase in the over-fitting due to less available training data (in each subdomain). That is, the domain decomposition of XPINNs can make a target function in a subdomain to be less complex than the whole target function, resulting in a reduction in a complexity measure, whereas each sub-network tend to utilize less than the entire available training data. To illustrate when and how XPINNs improve generalization based on our theory, we first provide analytical examples, where we mathematically compute and compare the prior bounds of XPINNs and PINNs. Furthermore, we adopt five PDEs to numerically demonstrate our posterior bounds via experiments. Both analytical examples and experimental observations confirm our theoretical prediction and deepen our understanding, demonstrating that the two factors in our generalization bounds lead to a tradeoff, leading to different performances of XPINNs over PINNs on various tasks.

The remainder of this paper is arranged as follows. In Section 2, we provide properties, background and assumptions on PDEs, PINNs, and the function space for multi-layer neural networks. In Section 3, our main generalization results (both prior and posterior bounds) are presented. In Section 4, discussion on theoretical analysis as well as analytical examples are introduced. In Section 5, extensive experiments are conducted to numerically demonstrate our theory.

2 Preliminaries

In this section, we present introductory facts for PDEs, neural networks, as well as PINNs and XPINNs. We use bold-faced lowercase letters to denote vectors, and capital letters to denote matrices and network parameters. Given a vector \mathbf{v} , we denote its Euclidean norm by $\|\mathbf{v}\|$, while $\|\cdot\|_p$ refers to the p -norms. For matrix norms, we denote the spectral norm by $\|\cdot\|$ and $l_{p,q}$ norms by $\|\mathbf{W}\|_{p,q} = (\sum_j (\sum_k |W_{j,k}|^p)^{q/p})^{1/q}$. Following convention, we define \inf of a set S to be the infimum of the subset S of $\overline{\mathbb{R}}$ (the set of affinely extended real numbers); e.g., the infimum of the empty set is infinity.

2.1 PDE Problem

In this paper, we consider PDEs defined on the bounded domain $\Omega = (-1, 1)^d$. More specifically, the PDEs under consideration are in the form of

$$\mathcal{L}u^* = f \text{ in } \Omega, \quad u^* = g \text{ on } \partial\Omega, \quad (1)$$

where \mathcal{L} is the differential operator characterizing the PDE, $\partial\Omega$ is the boundary of the set Ω , $f : \mathbf{x} = (x_1, \dots, x_d) \in \Omega \mapsto f(\mathbf{x}) \in \mathbb{R}$ and $g : \mathbf{x} = (x_1, \dots, x_d) \in \partial\Omega \mapsto g(\mathbf{x}) \in \mathbb{R}$ are given functions, and the function $u^* : \mathbf{x} = (x_1, \dots, x_d) \in \overline{\Omega} \mapsto u^*(\mathbf{x}) \in \mathbb{R}$ is the unknown solution of PDEs with its domain $\overline{\Omega} = \Omega \cup \partial\Omega$.

2.2 PINN and XPINN

In this subsection, we introduce neural network-based PDE solvers PINNs and XPINNs. Specifically, in PINNs we optimize neural networks via gradient-based algorithms to enable the network functions to satisfy the data and the physical laws governed by the PDEs. Given n_b boundary training points $\{\mathbf{x}_{b,i}\}_{i=1}^{n_b} \subset \partial\Omega$ and n_r residual training points $\{\mathbf{x}_{r,i}\}_{i=1}^{n_r} \subset \Omega$, we approximate the true PDE solution $u^* : \overline{\Omega} \mapsto \mathbb{R}$ by the PINN function u_θ parameterized by θ via minimizing the empirical loss composed of the boundary loss and the residual loss, as given below.

$$R_S(\theta) = \frac{1}{n_b} \sum_{i=1}^{n_b} |u_\theta(\mathbf{x}_{b,i}) - g(\mathbf{x}_{b,i})|^2 + \frac{1}{n_r} \sum_{i=1}^{n_r} |\mathcal{L}u_\theta(\mathbf{x}_{r,i}) - f(\mathbf{x}_{r,i})|^2, \quad (2)$$

where the first term is included to force the network to satisfy boundary conditions, while the second term forces the network to satisfy the physical laws described by the PDEs.

XPINN is an extension of PINN, obtained by decomposing the whole domain $\overline{\Omega}$ into several subdomains, mapped to several sub-PINNs. The continuity between each sub-nets is maintained via the interface loss function and the final solution of XPINN is the combination and ensemble of all sub-nets, where each of them is responsible for prediction

on one subdomain. More specifically, the original domain Ω is decomposed into N_D subdomains as $\Omega = \cup_{i=1}^{N_D} \Omega_i$. The loss of XPINN contains the sum of losses for the sub-nets, which consist of boundary loss and residual loss, plus the interface loss using points on $\partial\Omega_i \cap \partial\Omega_j$, where $i, j \in \{1, 2, \dots, N_D\}$ such that $\partial\Omega_i \cap \partial\Omega_j \neq \emptyset$ to maintain the continuity between the two sub-nets i and j . Mathematically, the XPINN loss for the i -th subdomain is

$$R_S^i(\boldsymbol{\theta}^i) + \lambda_I \sum_{i,j:\partial\Omega_i \cap \partial\Omega_j \neq \emptyset} R_I(\boldsymbol{\theta}^i, \boldsymbol{\theta}^j), \quad (3)$$

where $\lambda_I \geq 1$ is the weight controlling the strength of interface loss, $\boldsymbol{\theta}^i$ is the parameters for subdomain i , and each $R_S^i(\boldsymbol{\theta}^i)$ is the PINN loss for subdomain i containing boundary and residual losses, i.e.

$$R_S^i(\boldsymbol{\theta}^i) = \frac{1}{n_{b,i}} \sum_{j=1}^{n_{b,i}} |u_{\boldsymbol{\theta}^i}(\mathbf{x}_{b,j}^i) - g(\mathbf{x}_{b,j}^i)|^2 + \frac{1}{n_{r,i}} \sum_{j=1}^{n_{r,i}} |\mathcal{L}u_{\boldsymbol{\theta}^i}(\mathbf{x}_{r,j}^i) - f(\mathbf{x}_{r,j}^i)|^2, \quad (4)$$

where $n_{b,i}$ and $n_{r,i}$ are the number of boundary points and residual points in subdomain i respectively, $\mathbf{x}_{b,j}^i$ and $\mathbf{x}_{r,j}^i$ are the j -th boundary and residual training points in subdomain i , respectively. Moreover, $R_I(\boldsymbol{\theta}^i, \boldsymbol{\theta}^j)$ is the interface loss between the i -th and j -th subdomains based on several interface training points $\{\mathbf{x}_{I,k}^{ij}\}_{k=1}^{n_{I,ij}} \subset \partial\Omega_i \cap \partial\Omega_j$

$$R_I(\boldsymbol{\theta}^i, \boldsymbol{\theta}^j) = \frac{1}{n_{I,ij}} \sum_{k=1}^{n_{I,ij}} [|u_{\boldsymbol{\theta}^i}(\mathbf{x}_{I,k}^{ij}) - \{u_{\boldsymbol{\theta}^{avg}}\}|^2 + |(\mathcal{L}u_{\boldsymbol{\theta}^i}(\mathbf{x}_{I,k}^{ij}) - f_i(\mathbf{x}_{I,k}^{ij})) - (\mathcal{L}u_{\boldsymbol{\theta}^j}(\mathbf{x}_{I,k}^{ij}) - f_j(\mathbf{x}_{I,k}^{ij}))|^2], \quad (5)$$

where $\{u_{\boldsymbol{\theta}^{avg}}\} = u_{avg} := (u_{\boldsymbol{\theta}^i}(\mathbf{x}_{I,k}^{ij}) + u_{\boldsymbol{\theta}^j}(\mathbf{x}_{I,k}^{ij}))/2$, $n_{I,ij}$ is the number of interface points between the i -th and j -th subdomains, while $\mathbf{x}_{I,k}^{ij}$ is the k -th interface points between them. The first term is the average solution continuity between the i -th and the j -th sub-nets, while the second term is the residual continuity condition on the interface given by the i -th and the j -th sub-nets.

For our discussion on generalization, besides the training losses above, the testing loss evaluating generalization ability is defined as

$$R_D(\boldsymbol{\theta}) = \mathbb{E}_{\text{Unif}(\partial\Omega)} |u_{\boldsymbol{\theta}}(\mathbf{x}) - g(\mathbf{x})|^2 + \mathbb{E}_{\text{Unif}(\Omega)} |\mathcal{L}u_{\boldsymbol{\theta}}(\mathbf{x}) - f(\mathbf{x})|^2, \quad (6)$$

where $\text{Unif}(A)$ is the uniform distribution on a set A . Note that in the definition of the population loss, the interface losses of XPINNs are excluded to compare PINNs and XPINNs with the same quantity – the generalization bound for the boundary and residual terms. The beneficial effect of the interface loss is in improving the generalization of the boundary and residual terms instead of helping the generalization of the interface term itself. This is because the interface allows the sub-net in the subdomain Ω_i to implicitly use samples from other subdomain Ω_j ($i \neq j$) for regularization through the continuity.

Lastly, we denote the boundary empirical loss and the residual empirical loss by $R_{S\partial\Omega}$ and $R_{S\Omega}$, respectively, and their population versions by $R_{D\partial\Omega}$ and $R_{D\Omega}$, inspired by the fact that boundary points are on $\partial\Omega$ and that residual points are in Ω .

2.3 Neural Networks

In this subsection, we define neural networks and their related properties.

Definition 2.1. (Neural Network). A deep neural network (DNN) $u_{\boldsymbol{\theta}} : \mathbf{x} = (x_1, \dots, x_d) \in \overline{\Omega} \mapsto u_{\boldsymbol{\theta}}(\mathbf{x}) \in \mathbb{R}$, parameterized by $\boldsymbol{\theta}$ of depth L is the composition of L linear functions with element-wise non-linearity σ , is expressed as below.

$$u_{\boldsymbol{\theta}}(\mathbf{x}) = \mathbf{W}^L \sigma(\mathbf{W}^{L-1} \sigma(\dots \sigma(\mathbf{W}^1 \mathbf{x}))), \quad (7)$$

where $\mathbf{x} \in \mathbb{R}^d$ is the input, and $\mathbf{W}^l \in \mathbb{R}^{m_l \times m_{l-1}}$ is the weight matrix at l -th layer with $d = m_0$ and $m_L = 1$. The parameter vector $\boldsymbol{\theta}$ is the vectorization of the collection of all parameters.

We consider DNNs without bias because one can always set $\mathbf{x} \leftarrow [\mathbf{x}, 1]$ to involve the bias term. Note that the non-linearity σ is Lipschitz continuous with Lipschitz constant 1 in Ω . The widely adopted ReLU activation function $\text{ReLU}(\mathbf{x}) = \max(0, \mathbf{x})$ cannot be used in our setting due to its non-differentiability.

Because the neural network $u_{\boldsymbol{\theta}}$ is always differentiated with respect to its input in the residual losses in PINNs, we introduce their expressions as follows:

$$\frac{\partial u_{\boldsymbol{\theta}}(\mathbf{x})}{\partial \mathbf{x}} = \mathbf{W}^L \cdot \boldsymbol{\Phi}^{L-1} \mathbf{W}^{L-1} \dots \boldsymbol{\Phi}^1 \mathbf{W}^1 \in \mathbb{R}^d, \quad (8)$$

$$\frac{\partial^2 u_{\theta}(\mathbf{x})}{\partial \mathbf{x}^2} = \left\{ \sum_{l=1}^{L-1} (\mathbf{W}^L \Phi^{L-1} \dots \mathbf{W}^{l+1}) \text{diag}(\Psi^l \dots \Psi^1 \mathbf{W}_{:,j}^1) (\mathbf{W}^l \dots \Phi^1 \mathbf{W}^1) \right\}_{1 \leq j \leq d}, \quad (9)$$

where $\Phi^l = \text{diag}[\sigma'(\mathbf{W}^l \sigma(\mathbf{W}^{l-1} \sigma(\dots \sigma(\mathbf{W}^1 \mathbf{x}))))] \in \mathbb{R}^{m_l \times m_l}$, and $\Psi^l = \text{diag}[\sigma''(\mathbf{W}^l \sigma(\mathbf{W}^{l-1} \sigma(\dots \sigma(\mathbf{W}^1 \mathbf{x}))))] \in \mathbb{R}^{m_l \times m_l}$. In the Appendix, we provide detailed computation of the derivatives.

2.4 Generalized Barron Space

In this subsection, we introduce the generalized Barron space [17], which is a natural building block to construct a function space of multi-layer deep networks. This will facilitate our study of their approximation and generalization properties. We begin by presenting some mathematical background.

Let X be a Banach space such that X embeds continuously into the space $C^{0,1}(\Omega)$ of Lipschitz functions on Ω , and the closed unit ball B^X in X is closed in the topology of $C^0(\Omega)$. Because X embeds continuously into the space $C^{0,1}(\Omega)$, the Lipschitz constants of functions in B^X are bounded by the same constant and thus the subset B^X is (uniformly) equicontinuous. Recalling the Arzela-Ascoli theorem (stating that a subset of $C^0(\Omega)$ is pre-compact if and only if the subset is equicontinuous), the subset B^X is pre-compact (its closure is compact) in the separable Banach space $C^0(\Omega)$ (because Ω is compact). Since B^X is C^0 -closed and pre-compact, it is compact and is a Polish space in particular.

Let μ be a finite signed measure on the Borel σ -algebra of B^X (with respect to the C^0 -norm). Then μ is a signed Radon measure. We therefore consider the infinite-dimensional vector function version of the activation $\sigma : B^X \rightarrow C^0(\Omega)$ given by $\sigma : g \mapsto (\sigma \circ g)$ for each $g \in B^X$, where $(a \circ b)$ represents the composition of functions a and b . Then, the infinite-dimensional vector function σ is continuous due to the Lipschitz continuity of the dimensional wise version of σ . Thus, the infinite-dimensional vector function σ is strongly measurable (the preimage of Borel sets in B^X are Borel sets in $C^0(\Omega)$), and μ -integrable in the sense of the Bochner integral. The above construction of new function class containing all $\sigma \circ g$ from the class of g in B^X can be formalized as follows.

Definition 2.2. (*Generalized Barron Space*) *The generalized Barron space modeled on X associated with the non-linearity σ is a normed space $(\mathcal{B}_{X,\Omega}, \|\cdot\|_{X,\Omega})$ with*

$$\begin{aligned} \mathcal{B}_{X,\Omega} &= \{f \in C^0(\Omega) : \|f\|_{X,\Omega} < \infty\}, \text{ and} \\ \|f\|_{X,\Omega} &= \inf \{ \|\mu\|_{\mathcal{M}(B^X)} : \mu \in \mathcal{M}(B^X) \text{ s.t. } f = f_{\mu} \text{ on } \Omega \}, \end{aligned} \quad (10)$$

where $\mathcal{M}(B^X)$ denotes the space of Radon measures on B^X and $f_{\mu} = \int_{B^X} \sigma(g) d\mu(g)$. Here, the integral represents the Bochner integral with $g \in B^X$.

For example, if X is the space of linear functions from \mathbb{R}^d to \mathbb{R} (which is isomorphic to \mathbb{R}^{d+1}), then the generalized Barron space modeled on X is the (usual) Barron space for two-layer neural networks [18]. If X is the (usual) Barron space of two-layer neural networks, then the generalized Barron space modeled on X is the space for three-layer neural networks. That is, we can construct the generalized Barron space of L -layer networks from that of $(L-1)$ -layer networks by recursively applying its definition. This recursive construction leads to the *tree-like function space* (Definition 2.3), which is a function space of multi-layer neural networks (Theorem 2.1), as given below.

Definition 2.3. (*Tree-Like Function Space for Deep Networks*) *The tree-like function space $\mathcal{W}^L(\Omega)$ of depth L is recursively defined by $\mathcal{W}^l(\Omega) = \mathcal{B}_{\mathcal{W}^{l-1}(\Omega),\Omega}$ for all $l \in \{2, 3, \dots, L\}$ where $\mathcal{W}^1(\Omega)$ is the space of linear functions from \mathbb{R}^d to \mathbb{R} .*

Theorem 2.1. (*Embedding of Finite Networks*). *The tree-like function space $\mathcal{W}^L(\Omega)$ contains all finite multi-layer networks $u_{\theta}(\mathbf{x})$ of depth L satisfying $\|\mathbf{W}^l\|_{1,\infty} \leq 1, 1 \leq l \leq L-1$, and the Barron norm of networks satisfies $\|u_{\theta}\|_{\mathcal{W}^L(\Omega)} \leq \|\mathbf{W}^L\|_{1,\infty}$.*

Theorem 2.1 shows that the tree-like function space constructed via the generalized Barron space indeed contains the class of multi-layer neural networks, the norm of which is controlled by the $1, \infty$ matrix norm of their parameters. The following is a list of basic properties of the generalized Barron space, which also holds for the tree-like function space and justifies our recursive construction of the tree-like function space:

Theorem 2.2. (*Property of Generalized Barron Spaces*). *The following two statements are true. (1) The generalized Barron space is complete in the metric defined by the generalized Barron norm $\|\cdot\|_{X,\Omega}$: i.e., the generalized Barron space is a Banach space. (2) $\mathcal{B}_{X,\Omega}$ embeds continuously into $C^{0,1}(\Omega)$ and the closed unit ball of $\mathcal{B}_{X,\Omega}$ is a closed subset of $C^0(\Omega)$.*

The last property indicates that $\mathcal{B}_{X,\Omega}$ satisfies the same properties, which we imposed on X during the construction, i.e., we can repeat the construction and consider $\mathcal{B}_{\mathcal{B}_{X,\Omega}}$, hence, ensuring the validity of the recursive construction in the tree-like function space. As universal approximators, neural networks can also approximate arbitrary Barron functions accurately.

Theorem 2.3. (*Approximation Properties of Tree-Like Functions*). *Let \mathbb{P} be a probability measure with compact support in Ω . Then for any $L \geq 1$, $f \in \mathcal{W}^L(\Omega)$ and $m \in \mathbb{N}$, there exists a neural network $u_\theta(\mathbf{x}; \theta)$ of depth L in equation (7), with width $m_l = m^{L-l+1}$, $\forall l > 1$ such that $\|u_m - f\|_{L^2(\mathbb{P})} \leq 3L\|f\|_{\mathcal{W}^L(\Omega)}/\sqrt{m}$, with $\|\theta\|_{\mathcal{P}} \leq \|\mathbf{W}^L\|_{1,\infty} \leq \|f\|_{\mathcal{W}^L(\Omega)}$, where $\|\cdot\|_{\mathcal{P}}$ is the path norm defined as $\|\theta\|_{\mathcal{P}} = \sum_{i_L} \cdots \sum_{i_0} |\mathbf{W}_{i_L}^L \cdots \mathbf{W}_{i_1 i_0}^1|$.*

The path norm is one type of complexity measure of neural networks correlated to generalization [19]. The above theorem shows that the neural networks can approximate any target function in the generalized Barron space well with complexities controlled by the Barron norm of the target functions, which shows the efficiency of network approximation. This is utilized in the proof of our prior generalization bound in Theorem 3.1.

3 Theory

In this section, we introduce our main generalization results, including a prior bound based on the Barron space and a posterior bound based on the Rademacher complexity. For both of them, we use the following assumption adopted from a closely related previous study [13].

Assumption 3.1. (*Symmetry and boundedness of \mathcal{L}*). *Throughout the analysis in this paper, we assume the differential operator \mathcal{L} in the PDE satisfies the following conditions. The operator \mathcal{L} is a linear second-order differential operator in a non-divergence form, i.e., $(\mathcal{L}u^*)(\mathbf{x}) = \sum_{\alpha=1}^d \sum_{\beta=1}^d \mathbf{A}_{\alpha\beta}(\mathbf{x})u_{x_\alpha x_\beta}^*(\mathbf{x}) + \sum_{\alpha=1}^d \mathbf{b}_\alpha(\mathbf{x})u_{x_\alpha}^*(\mathbf{x}) + c(\mathbf{x})u^*(\mathbf{x})$, where all $\mathbf{A}_{\alpha\beta}, \mathbf{b}_\alpha, c : \Omega \rightarrow \mathbb{R}$ are given coefficient functions and $u_{x_\alpha}^*$ are the first-order partial derivatives of the function u^* with respect to its α -th argument (the variable x_α) and $u_{x_\alpha x_\beta}^*$ are the second-order partial derivatives of the function u^* with respect to its α -th and β -th arguments (the variables x_α and x_β). Furthermore, there exists K such that for all $\mathbf{x} \in \Omega = [-1, 1]^d$, and $\alpha, \beta \in [d]$, we have $A_{\alpha\beta} = A_{\beta\alpha}$ and $|A_{\alpha\beta}(\mathbf{x})| \leq K$, $|b_\alpha(\mathbf{x})| \leq K$, $|c(\mathbf{x})| \leq K$.*

Because multiplying the network functions by the coefficients $\mathbf{A}, \mathbf{b}, c$ and differentiation on them influence their complexities, the universal bound on the coefficients $\mathbf{A}, \mathbf{b}, c$ and the restriction to second order PDEs are required for our estimation on the Rademacher complexity of the hypothesis class of PINNs.

3.1 A Prior Generalization Bound (Theorem 3.1)

In this subsection, we introduce our prior bound based on the Barron space, beginning with the following assumption, which is only used in Theorem 3.1 and *not* required in Theorem 3.2:

Assumption 3.2. (*Regularity of the PDE*). *For any training dataset S and network $u_\theta(\mathbf{x})$ such that $R_D(u_\theta(\mathbf{x}) - u^*(\mathbf{x}))^2 \leq \epsilon$ for some $\epsilon > 0$, there exists a universal constant $C_{pde} \geq 1$, which depends on the PDE problem and the neural network, such that $R_{S \cap \Omega}(\mathcal{L}u_\theta(\mathbf{x}) - \mathcal{L}u^*(\mathbf{x}))^2 \leq C_{pde}\epsilon$.*

This assumption states that if the neural network approximates the solution sufficiently well in L^2 norm, then its differentiation is also close to the differentiation of the PDE solution.

We assume that the constant C_{pde} depends on the neural network (e.g., its derivatives) due to the differentiated net in the residual loss. The following theorem states our prior generalization bound.

Theorem 3.1. (*A prior generalization bound on PINN*). *Let the Assumptions given in 3.1 and 3.2 hold, then for any $\delta \in (0, 1)$ and the depth L , suppose that the true solution $u^*(\mathbf{x})$ lies in the tree-like function space $\mathcal{W}^L(\Omega)$ and $\lambda = 9C_{pde}^2 L^2/m$. Let $\theta_{S,\lambda} = \arg \min_{\theta} J_{S,\lambda}(\theta) = R_S(\theta) + \lambda\|\theta\|_{\mathcal{P}}^2$. Then, with probability at least $1 - \delta$ over the choice of random samples $S = \{\mathbf{x}_i\}_{i=1}^{n_b+n_r} \subset \bar{\Omega}$ with n_b boundary points and n_r residual points, we obtain the following generalization bound*

$$\begin{aligned} R_{\mathcal{D} \cap \partial\Omega} &\leq R_{S \cap \partial\Omega} + 4\sqrt{2}\|u^*\|_{\mathcal{W}^L(\Omega)}\sqrt{(L+1+\log(d))/n_b} + c\sqrt{2\log(2/\delta)/n_b}. \\ R_{\mathcal{D} \cap \Omega} &\leq R_{S \cap \Omega} + 4\sqrt{2}Kd(L+1)\|u^*\|_{\mathcal{W}^L(\Omega)}\sqrt{(L+1+\log(d))/n_r} + c\sqrt{2\log(2/\delta)/n_r}. \end{aligned} \quad (11)$$

In Theorem 3.1, the generalization bounds on the right-hand side of equation (11) (for both the boundary and the residual points) contain three terms, where the first term is the empirical training loss, the second term is the complexity of the model (original network for boundary loss and differentiated network for residual loss), and the third term is the statistical term. Moreover, this theorem shows that under certain regularization of the path norm, the generalization

errors of PINNs are controlled by the Barron norm of the target function u^* . If the target function u^* is more complex (simpler), i.e., it has larger (smaller) Barron norm, the generalization error will be larger (smaller). This reflects a data-dependent bound in which neural networks control their complexity based on those of target functions. The above advantages are also summarized in the appendix to justify our choice of Barron space.

Finally, we note that Assumption 3.2 is indispensable for Theorem 3.1 (although it is *not* used in Theorem 3.2) and it is used to transfer the empirical loss containing boundary and residual losses into an L^2 approximation error between the network and u^* during the proof.

3.2 A Posterior Generalization Bound (Theorem 3.2)

We now provide a *posterior* generalization bound based on the *optimized* network parameters (which are obtained after optimization). We begin by defining the Rademacher complexity [20], which is one of key notions in statistical learning theory.

Definition 3.1. (*Rademacher Complexity*). Let $S = \{x_i\}_{i=1}^n \subset \bar{\Omega}$ be a dataset containing n samples. The Rademacher complexity of a function class \mathcal{F} on S is defined as $\text{Rad}(\mathcal{F}; S) = \mathbb{E}_\epsilon \left[\sup_{f \in \mathcal{F}} \frac{1}{n} \sum_{i=1}^n \epsilon_i f(x_i) \right]$, where $\epsilon_1, \dots, \epsilon_n$ are independent and identically distributed (i.i.d.) random variables taking values uniformly in $\{-1, 1\}$.

Intuitively, Rademacher complexity measures the richness of function class \mathcal{F} by studying its ability to fit random labels of x_i generated by ϵ_i . Since simpler function classes tend to generalize better on unseen testing data, we will investigate the Rademacher complexities of PINNs and XPINNs, which begins with a key lemma on that of neural networks.

Lemma 3.1. (*Rademacher Complexity of Neural Networks*). For every L , and every set of n points $S \subset \bar{\Omega}$, the hypothesis class \mathcal{NN}_M^L given by the neural networks

$$\mathcal{NN}_M^L := \left\{ u_\theta(\mathbf{x}) = \mathbf{W}^L \sigma(\mathbf{W}^{L-1} \sigma(\dots \sigma(\mathbf{W}^1 \mathbf{x}))) \mid \|\mathbf{W}^l\|_{1,\infty} \leq M(l), \forall l \right\}, \quad (12)$$

satisfies the Rademacher complexity bound

$$\text{Rad}(\mathcal{NN}_M^L; S) \leq 2 \prod_{l=1}^L M(l) \sqrt{\frac{L+1+\log(d)}{n}}. \quad (13)$$

This lemma controls Rademacher complexities of neural networks by the product of the $1, \infty$ norms of the network parameter matrices at each layer. The complexity depends mildly on the network depth via the $\sqrt{L+1+\log(d)}$ term. We extend this result to the differentiated PINNs in the following lemma.

Lemma 3.2. (*Rademacher Complexity of Differentiated Networks*). For every L , and every set of n points $S \subset \bar{\Omega}$, the hypothesis class $\mathcal{PINN}_M^L = \{\mathcal{L}u \mid u \in \mathcal{NN}_M^L\}$, satisfies the Rademacher complexity bound

$$\text{Rad}(\mathcal{PINN}_M^L; S) \leq 2K[1 + M(1) + d(L-1)M(1)^2] \prod_{l=1}^L M(l) \sqrt{\frac{L+1+\log(d)}{n}}. \quad (14)$$

This lemma shows a similar Rademacher complexity bound for PINNs, where the main differences are in the $M(1)$ and $M(1)^2$ terms, which are due to the first order and second order differentiation in PINNs, respectively. Using these lemmas, we derive the following posterior generalization bound.

Theorem 3.2. (*A posterior generalization bound on PINN*). Let Assumptions 3.1 hold, for any $\delta \in (0, 1)$ and the depth L , let the (not regularized) empirical loss function be $\theta_S = \arg \min_{\theta} R_S(\theta)$. Then, with probability at least $1 - \delta$ over the choice of random samples $S = \{x_i\}_{i=1}^{n_b+n_r} \subset \bar{\Omega}$ with n_b boundary points and n_r residual points, we have the following generalization bound

$$\begin{aligned} |R_{D \cap \partial \Omega}(\theta) - R_{S \cap \partial \Omega}(\theta)| &\leq 2(N+1)^2 \tau(n_b) \\ |R_{D \cap \Omega}(\theta) - R_{S \cap \Omega}(\theta)| &\leq 2K^2 d^2 (L+1)^2 (N+1)^2 \tau(n_r). \end{aligned} \quad (15)$$

where $\tau(n) = 2\sqrt{(L+1+\log(d))/n} + \sqrt{\log(\pi^2(N+1)^2/3\delta)/(2n)}$, $M(l) = \|\mathbf{W}^l\|_{1,\infty}$, and

$$N = \max \left[\prod_{l=1}^L M(l), M(1) \prod_{l=1}^L M(l), M(1)^2 \prod_{l=1}^L M(l), M(L) \right]. \quad (16)$$

The generalization bounds are mainly controlled by the complexity of networks measured by $\{M(l)\}_{l=1}^L$ and the corresponding N quantities, as well as the last statistical term. When compared to the prior bound in Theorem 3.1, the posterior bound in Theorem 3.2 is easier to compute numerically, because it only involves terms related to neural network parameters. Despite the difference, Theorems 3.1 and 3.2 are related. Concretely, Theorem 3.1 shows that if the target function u^* is more complex (simpler), i.e., has larger (smaller) Barron norm, the generalization error is larger (smaller), which implies that a complex (simple) neural network has been learnt to fit the target since complex (simple) network generalizes worse (better). On the other hand, the complexity of neural networks can also be reflected by the quantities $\{M(l)\}_{l=1}^L$ and N in Theorem 3.2 [19] since they are directly linked to Rademacher complexity in Lemmas 3.1 and 3.2. Hence, we can expect that PINNs learning more complex target functions have larger $\{M(l)\}_{l=1}^L$ and N quantities. And if a trained PINN has large $\{M(l)\}_{l=1}^L$ and N quantities, which signifies higher complexity, the target function fitted should also be complicated (i.e., it has a larger Barron norm) due to the implicit regularization of network training, i.e., stochastic gradient training finds out complex (simple) solution given a complex (simple) target.

3.3 Comparing XPINN and PINN by Theorem 3.1

In this subsection, we compare PINNs with XPINNs by using the generalization bound in Theorem 3.1. We focus on comparing PINN with XPINN on the residual loss, i.e. $R_{D \cap \Omega}$ and $R_{S \cap \Omega}$, because it is more representative of the differentiated nets in PINNs. The case for boundary loss is similar but simpler, which is included in the Appendix. Specifically, the comparison is performed by computing their respective theoretical bounds. In particular, the generalization performance of PINN depends on the upper bound in Theorem 3.1, which is: $R_{S \cap \Omega} + 4\sqrt{2}Kd(L+1)\|u^*\|_{\mathcal{W}^L(\Omega)}\sqrt{(L+1+\log(d))/n_r} + c\sqrt{2\log(2/\delta)}/n_r$, where n_r is the number of residual training points.

For XPINN's generalization, we can apply Theorem 3.1 to each of the subdomains in the XPINN. Specifically, for the i -th sub-net in the i -th subdomain of XPINN, i.e., the $\Omega_i, i \in \{1, 2, \dots, N_D\}$, its generalization performance is upper bounded by $R_{S \cap \Omega_i} + 4\sqrt{2}Kd(L+1)\|u^*\|_{\mathcal{W}^L(\Omega_i)}\sqrt{(L+1+\log(d))/n_{r,i}} + c\sqrt{2\log(2/\delta)}/n_{r,i}$, where $n_{r,i}$ is the number of training boundary points in the i -th subdomain.

Hence, since the i -th subdomain has $n_{r,i}$ training boundary points and is in charge of the prediction of $\frac{n_{r,i}}{n_r}$ proportion of testing data, we weight-averaged their generalization errors to get the generalization error of XPINN: $\sum_{i=1}^{N_D} \frac{n_{r,i}}{n_r} (R_{S \cap \Omega_i} + 4\sqrt{2}Kd(L+1)\|u^*\|_{\mathcal{W}^L(\Omega_i)}\sqrt{(L+1+\log(d))/n_{r,i}} + c\sqrt{2\log(2/\delta)}/n_{r,i})$. If we omit the last term and assume that their empirical losses are similar, i.e., $R_{S \cap \Omega} \approx \sum_{i=1}^{N_D} (n_{r,i}/n_r) R_{S \cap \Omega_i}$, and $c\sqrt{2\log(2/\delta)}/n_{r,i} \ll \|u^*\|_{\mathcal{W}^L(\Omega)}, \|u^*\|_{\mathcal{W}^L(\Omega_i)}$, then comparing the generalization ability of PINN and XPINN reduces to the following:

$$\|u^*\|_{\mathcal{W}^L(\Omega)}(\text{PINN}) \quad \text{versus} \quad \sum_{i=1}^{N_D} \sqrt{n_{r,i}/n_r} \|u^*\|_{\mathcal{W}^L(\Omega_i)}(\text{XPINN}), \quad (17)$$

where the model having smaller corresponding quantity is more generalizable.

In the next section, we will present three analytic examples and adopt the above comparison method to illustrate the circumstances under which XPINN is better or worse than PINN.

3.4 Comparing XPINN and PINN by Theorem 3.2

The comparison using Theorem 3.2 is also done via computing their respective theoretical bounds. The residual loss is considered in the main text while the case for boundary loss is included in the supplementary material. Concretely, we denote the upper bound of PINN testing loss as B_{PINN} and those of the sub-net i in XPINN as $B_{i,\text{XPINN}}$, $i \in \{1, 2, \dots, N_D\}$, which are provided by the right sides of Theorem 3.2, i.e., the bounds are $B_{\text{PINN}} = 2K^2d^2(L+1)^2(N+1)^2 \left(2\sqrt{(L+1+\log(d))/n_r} + \sqrt{\log(\pi^2(N+1)^2/3\delta)/(2n_r)} \right)$, and $B_{i,\text{XPINN}} = 2K^2d^2(L+1)^2(N_i+1)^2 \left(2\sqrt{(L+1+\log(d))/n_{r,i}} + \sqrt{\log(\pi^2(N_i+1)^2/3\delta)/(2n_{r,i})} \right)$, where n_r is the total number of residual training samples, $M(l) = \|\mathbf{W}^l\|_{1,\infty}$ where \mathbf{W}^l is the l -th layer weight matrix of the PINN model, and N is defined in Theorem 3.2 by the parameters \mathbf{W}^l , which is directly linked to Rademacher complexity of PINNs. Moreover, $n_{r,i}$ is the number of residual training samples in subdomain i , and $M_i(l) = \|\mathbf{W}_i^l\|_{1,\infty}$ where \mathbf{W}_i^l is the l -th layer weight matrix of the i -th sub-net in the XPINN model, and $N_i = \max[\prod_{l=1}^L M_i(l), M_i(1) \prod_{l=1}^L M_i(l), M_i(1)^2 \prod_{l=1}^L M_i(l), M_i(L)]$ is the N quantity for the i -th sub-net which measures the Rademacher complexity of the i -th sub-net. Because the i -th sub-net in XPINN is in charge of the prediction of $\frac{n_{r,i}}{n_r}$ proportion of testing data, we weight-averaged their bounds to get that of XPINN, i.e., $B_{\text{XPINN}} = \sum_{i=1}^{N_D} (n_{r,i}/n_r) B_{i,\text{XPINN}}$ where B_{XPINN} is the bound for XPINN. Thus, we only need to compare B_{PINN} with B_{XPINN} , where the model having smaller corresponding quantity is more generalizable. These quantities can be directly measured and calculated from the trained deep nets, which allows for easy numerical validation. Thus, we validate this comparison method in computational experiments.

4 Analytical Examples Based on Theorem 3.1

In this section, we provide analytical examples to further analyze the prior generalization bound in Theorem 3.1. The examples ensure analytical expressions of the Barron norm, which results in precise calculation of prior bounds. Specifically, we show in what cases XPINNs are better than, similar to, and worse than PINNs in order to demonstrate the tradeoff in XPINN generalization.

4.1 Case where XPINN Outperforms PINN

Let us consider the target function $u^*(x, y) = 2 \sin x + \sin y$, on the broken line $\Omega = \Omega_1 \cup \Omega_2 = [0, 1] \times \{0\} \cup \{0\} \times [0, 1]$. Obviously, we have $\|u^*\|_{\mathcal{W}^2(\Omega)} = 3$, recall that $\mathcal{W}^2(\Omega)$ is the natural function space of two-layer sine networks on Ω . Interestingly, if we restrict $u^*(x, y)$ to Ω_1 , we have $u^*(x, y) = 2 \sin x$ on Ω_1 , with a Barron norm $\|u^*\|_{\mathcal{W}^2(\Omega_1)} = 2$. Similarly, if we restrict our observation to Ω_2 , we have $\|u^*\|_{\mathcal{W}^2(\Omega_2)} = 1$. Since the lines Ω_1 and Ω_2 have the same length, it is natural to assume that the numbers of train residual data points on Ω_1 and Ω_2 are the same, i.e. $n_{r,1} = n_{r,2} = n_r/2$ in equation (17). We compare a PINN on Ω and an XPINN with two sub-nets on Ω_1 and Ω_2 , respectively. Applying Theorem 3.1 and our discussion in section 3.1, $3 = \|u^*\|_{\mathcal{W}^2(\Omega)} \leq (\|u^*\|_{\mathcal{W}^2(\Omega_1)} + \|u^*\|_{\mathcal{W}^2(\Omega_2)})/\sqrt{2} = (2 + 1)/\sqrt{2} = 3/\sqrt{2}$. Thus, XPINN generalizes better than PINN.

The underlying reason is as follows: u^* remains simple on Ω_2 , while being complex on Ω_1 . Since XPINN optimizes several sub-nets at different subdomains, XPINN may learn a simple network on Ω_2 where the solution is simpler, (i.e., very small $\|u^*\|_{\mathcal{W}^2(\Omega_2)} = 1$). Also, it learns a complex network in other subdomains, where the solution is relatively complicated, (i.e., relatively large $\|u^*\|_{\mathcal{W}^2(\Omega_1)} = 2$). Therefore, compared with PINN, which learns a very complex network on the whole domain Ω (extremely large $\|u^*\|_{\mathcal{W}^2(\Omega)} = 3$), XPINN tends to have lower overall complexity, because it is complex on only part of the domain and remains simple on the rest of the domain, which leads to better generalization.

4.2 Case where XPINN is Worse Than PINN

Let us consider the same target function $u^*(x, y) = 2 \sin x + \sin y$, on a different broken line $\Omega = \Omega_1 \cup \Omega_2$, where $\Omega_1 = [0, 1] \times \{0\}$ and $\Omega_2 = \{(x, y) | y = x, x \in [0, \sqrt{2}/2]\}$. Obviously, we have $\|u^*\|_{\mathcal{W}^2(\Omega)} = 3$. Moreover, if we restrict $u^*(x, y)$ to Ω_1 , we have $u^*(x, y) = 2 \sin x$ on Ω_1 , with a Barron norm $\|u^*\|_{\mathcal{W}^2(\Omega_1)} = 2$. However, even if we restrict our observation to Ω_2 , we still have $\|u^*\|_{\mathcal{W}^2(\Omega_2)} = 3$. Since the lines Ω_1 and Ω_2 have the same length, it is natural to assume that the numbers of train residual data points on Ω_1 and Ω_2 are the same, i.e. $n_{r,1} = n_{r,2} = n_r/2$ in equation (17). We compare a PINN on Ω and an XPINN with two sub-nets on Ω_1 and Ω_2 respectively. Applying Theorem 3.1 and following our discussion in section 3.1, we have $3 = \|u^*\|_{\mathcal{W}^2(\Omega)} \leq (\|u^*\|_{\mathcal{W}^2(\Omega_1)} + \|u^*\|_{\mathcal{W}^2(\Omega_2)})/\sqrt{2} = (2 + 3)/\sqrt{2} = 5/\sqrt{2} \approx 3.53$. Thus, in this example XPINN is worse than PINN.

Although XPINN decreases the target function complexity via decomposition, at least on Ω_1 it decreases to 2 from 3, it cannot complement the overfitting of less available training data on generalization, which is reflected in the $\sqrt{1/n_r}$ term in the bound, where n_r is the number of residual training samples, i.e. the complexity grows with less data. Unfortunately, in this example, the more complexity brought by overfitting due to less data exceeds the benefit of simpler target function parts after decomposition. Hence, XPINN performs worse than PINN.

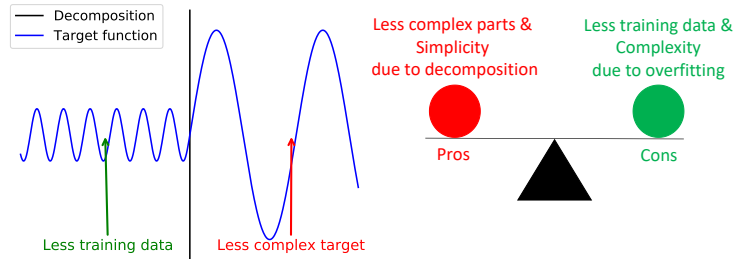


Figure 1: Left: Decomposition causes simpler target in each part (red), but less training data leads to overfitting. Right: Tradeoff between the two factors.

4.3 Illustration of a Tradeoff in XPINN generalization

In this section, we summarize the above two examples and derive a tradeoff in XPINN generalization, which is illustrated in Figure 1. There are two factors that counter-balance each other to affect XPINN generalization, namely the simplicity of decomposed target function within each subdomain thanks to domain decomposition, and the

complexity and inclination to overfit due to less available training data, which counter-balance each other as follows. When the former is more dominant, XPINN outperforms PINN, as in our example in section 4.1. Otherwise, PINN outperforms XPINN, as in our example in section 4.2. When the two factors reach a balance, XPINN and PINN perform similarly.

To make the idea clearer, we consider another analytical example. Let us consider the target function $u^*(x, y) = 2 \sin x + q \sin y$, on the broken line $\Omega = \Omega_1 \cup \Omega_2$, where $\Omega_1 = [0, 1] \times \{0\}$ and $\Omega_2 = \{(x, y) | y = x, x \in [0, \sqrt{2}/2]\}$, where $q \in \mathbb{R}^+$ is a fixed constant to be decided. Obviously, we have $\|u^*\|_{\mathcal{W}^2(\Omega)} = 2 + q$. Further, if we restrict $u^*(x, y)$ to Ω_1 , we have $u^*(x, y) = 2 \sin x$ on Ω_1 , with a Barron norm $\|u^*\|_{\mathcal{W}^2(\Omega_1)} = 2$. However, even if we restrict our observation to Ω_2 , we still have $\|u^*\|_{\mathcal{W}^2(\Omega_2)} = 2 + q$. Because the lines Ω_1 and Ω_2 have the same length, it is natural to assume that the numbers of train residual data points on Ω_1 and Ω_2 are the same, i.e. $n_{r,1} = n_{r,2} = n_r/2$ in equation (17). We compare a PINN on Ω and an XPINN with two sub-nets on Ω_1 and Ω_2 , respectively. Applying Theorem 3.1 and following our discussion in Section 3.1, we need to compare the following quantities to determine when XPINN outperforms PINN: $3 = \|u^*\|_{\mathcal{W}^2(\Omega)}$ versus $(\|u^*\|_{\mathcal{W}^2(\Omega_1)} + \|u^*\|_{\mathcal{W}^2(\Omega_2)})/\sqrt{2} = 2 + 2 + q/\sqrt{2} = 4 + q/\sqrt{2}$. When $q > 3\sqrt{2} - 4$, PINN is better due to its more obvious effect with less data. When $q < 3\sqrt{2} - 4$, XPINN performs better due to the more obvious effect by decomposing complexity into simplicity.

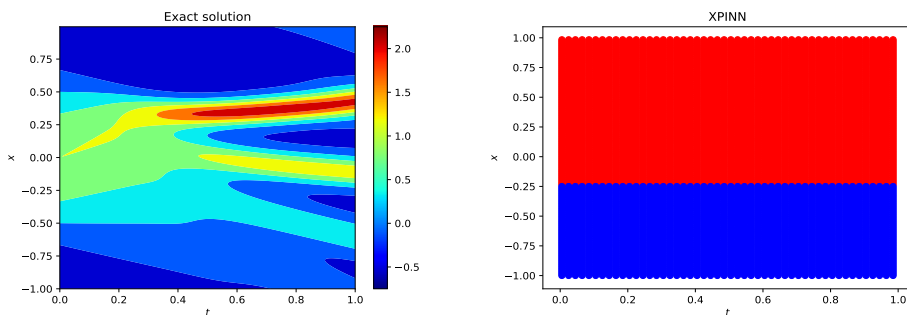


Figure 2: Left: Visualization of the exact solution of KdV equation. Right: domain decomposition in XPINN.

In summary, inspired by the two analytical examples, we have shown in this section that there exists a tradeoff in XPINNs, which results in their different performance when compared to PINNs. We further demonstrate these phenomena in computational experiments for various PDEs in the next section.

5 Computational Experiments

In the previous section, we presented the main idea of the generalization tradeoff by using the analytical examples based on the prior bound. In this section, we conduct extensive experiments to numerically demonstrate our posterior generalization results for PINNs and XPINNs. Specifically, we use five PDEs to show the cases where XPINNs are worse than and better than PINNs. Furthermore, even for the same PDE problem, we design different domain decomposition methods to show good and bad cases for XPINNs. Accordingly, we also discuss how to properly partition domains for XPINNs.

5.1 KdV Equation

5.1.1 Setup

In this experiment, we consider a one-dimensional KdV equation given by $u_t + uu_x = 0.0025u_{xxx}$, $x \in [-1, 1]$, $t \in [0, 1]$, with the boundary condition of $u(x, 0) = \cos(\pi x)$, $x \in [-1, 1]$. The true solution is visualized in Figure 2 left. The entire dataset for this PDE is provided by the paper of PINN [6].

The training dataset for PINN contains 6400 residual points and 128 boundary points, and both are uniformly distributed. The testing dataset for PINN contains 102400 points uniformly distributed within the domain. The backbone model for PINN is a 5-layer neural network with 20 hidden units activated by sine as in our theory. Adam [21] optimizer with $1e-3$ learning rate is used for optimization. No regularization is used.

Moreover, from the solution of the KdV equation in Figure 2 left, we observe that it is complex, and it fluctuates when $x \geq 0$ corresponding to the upper part. In contrast, the bottom part is smoother and simpler. Hence, to reflect our discussion on the prior bound and analytical examples, for XPINN we partition the whole domain into two subdomains, including (1) the top domain, corresponding to sub-net named XPINN-T as $x > -0.25$ and (2) the bottom domain,

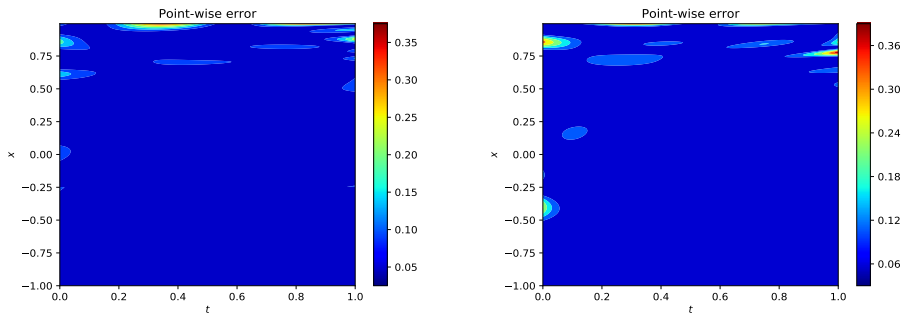


Figure 3: Left: Error visualization of XPINN. Right: Error visualization of PINN.

Table 1: Computational results for KdV equation.

Method	Training Loss	Testing Loss	Norms	Theoretical Bound
PINN	$2.227\text{e-}2 \pm 3.291\text{e-}3$	$2.352\text{e-}2 \pm 3.501\text{e-}3$	100.00%	100.00%
XPINN-T	$2.683\text{e-}2 \pm 3.320\text{e-}3$	$2.258\text{e-}2 \pm 2.896\text{e-}3$	85.10%	94.95%
XPINN-B			26.10%	

corresponding to sub-net named XPINN-B as $x \leq -0.25$. Then, the target function in subdomain 1 is complicated and it fluctuates significantly, while that in subdomain 2 is simpler and smoother.

The training and testing datasets for XPINN are the same as those for PINN for fair comparison. In other words, the training and testing data of each sub-net are points lying in the corresponding subdomain. The backbone models for XPINN are two 5-layer neural networks with 20 hidden units activated by sine as in our theory. Two Adam [21] optimizers with $1\text{e-}3$ learning rates are used for optimizations. No regularization is used.

Lastly, we need to pay attention to the choice of δ in the posterior bound. Because the bound in Theorem 3.2 holds with probability $1 - \delta$, in the computations we take $\delta = 0.1$ so that the bound holds with probability 0.9. At the same time, for XPINN, we need to take $\delta = 0.05$ because there are two sub-nets for a union bound.

5.1.2 Results

We present the experimental results including training and testing losses, as well as the calculated theoretical generalization bound in XPINN and PINN models in Table 1. Moreover, we also provide the product of norms of the neural network parameter matrices, which is directly linked to the Rademacher complexity of neural networks and thus their complexities (see Lemma 3.1). We compute this quantity to provide an intuitive observation on the complexities of the optimized neural networks.

The results show that XPINN generalizes much better than PINN, since XPINN has a larger training loss but smaller testing loss than PINN. The testing loss of XPINN is even smaller than its training loss, which is not contradictory because the error of XPINN concentrates in small areas within the domain (Figure 3 left). Since the testing points are denser than training points, the majority of the former are in areas with smaller errors, which leads to a smaller testing loss.

In addition, the products of norms of the weight matrices are presented in the columns “Norms” where that of PINN is denoted 100% for clear comparison. The complexity of PINN is the largest, since PINN has to fit the entire target function into one network, which is very complex. In contrast, the complexities of sub-nets in XPINN are smaller, which may be attributed to the fact that domain decomposition divides the complicated target function into two simpler ones. For the two sub-nets in XPINN, sub-net 1 is more complex than sub-net 2, where the former corresponds to the domain $x > -0.25$, where the solution is more complicated and the latter corresponds to the simpler domain, validating the implicit regularization of gradient descent, which learns simple (complex) function with simple (complex) neural networks.

Furthermore, the “Bound” columns in Table 1 are the theoretical generalization bounds for PINN and XPINN, where that of PINN is denoted as 100% for clarity. The theoretical generalization bound of XPINN is 94.95%, which is lower than PINN and consistent with their testing performances, justifying the effectiveness of our generalization bound. The reason for better generalization may lie in the simplicity due to the decomposition. Specifically, the complexities of the two sub-nets are reduced to only 85.10% and 26.10%, whose positive effects are more obvious than the overfitting due to less data during training each sub-net.

In conclusion, for the KdV equation, the positive effect of simplicity of target functions in every subdomain

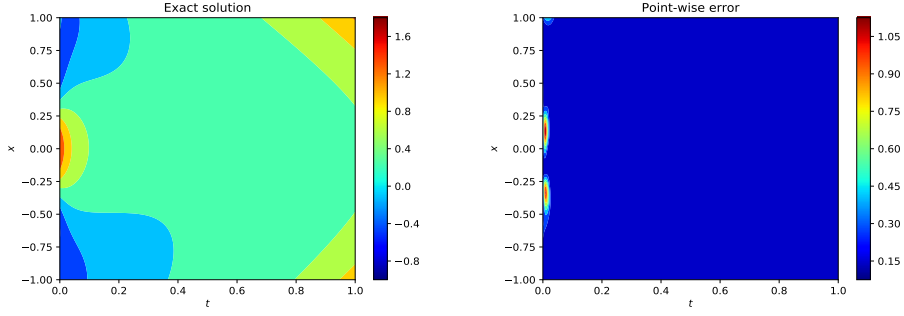


Figure 4: Left: exact solution of the heat equation. Right: error visualization of XPINN-LR.

Table 2: Computational results for heat equation.

Method	Train Loss	Test Loss	Norms	Theoretical Bound
PINN	$8.984e-3 \pm 1.939e-3$	$1.116e-2 \pm 1.951e-3$	100.00%	100.00%
XPINN-L	$7.896e-3 \pm 1.770e-3$	$8.799e-3 \pm 2.072e-3$	79.54%	59.68%
XPINN-R			41.94%	
XPINN-T	$7.397e-3 \pm 1.982e-3$	$1.100e-2 \pm 2.209e-3$	73.03%	110.44%
XPINN-B			76.04%	

brought by the domain decomposition is more obvious than the overfitting effect caused by less available data in each subdomain, which leads to better performance of XPINN than PINN overall.

5.2 Heat Equation

5.2.1 Setup

In this subsection, we consider the heat equation, which is a second order linear PDE. The one-dimensional heat equation under consideration is $u_t = u_{xx}$, $x \in [-1, 1]$, $t \in [0, 1]$, with the boundary conditions given by the true solution

$$u(x, t) = e^{-\pi^2 t} \cos(\pi x) + 0.6e^{-4\pi^2 t} \cos(2\pi x) + 0.3e^{4t-4} \cosh(2x) + 0.1e^{t-1} \sinh x. \quad (18)$$

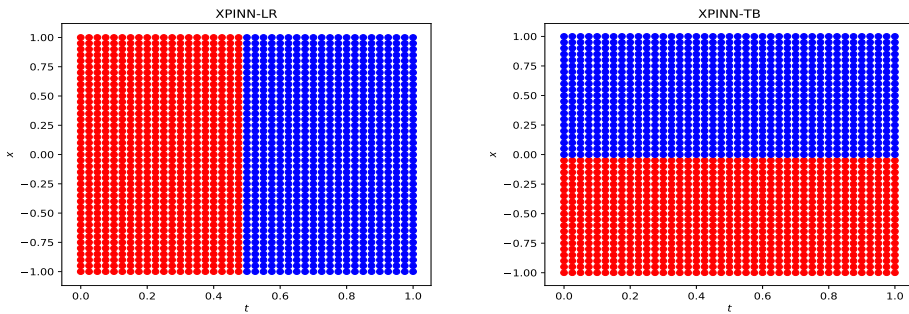


Figure 5: Domain partition in the XPINN of heat equation. Left: XPINN-LR, right: XPINN-TB.

The solution is visualized in Figure 4 left. The training dataset for PINN contains 1681 residual points and 81 boundary points, whereas the testing dataset for PINN contains 160801 points within the domain. The backbone model for PINN is a 8-layer neural network with 20 hidden units activated by sine. Adam [21] with $1e-3$ learning rate is used. No regularization is used.

For domain decomposition of XPINN, from Figure 4 left, we observe that the solution of heat equation is complex near $t = 0$ and $t = 1$, due to the two nearby heat sources. The two heat sources are also dissimilar: at $t = 0$ the source is generated by trigonometric functions, while at $t = 1$ it is generated by hyperbolic functions. To design a good XPINN, we should partition the complexities of the two heterogeneous heat sources into different subdomains. Thus, in XPINN-LR shown in Figure 5 left, we partition the whole domain into a left domain $t \leq 0.5$ containing trigonometric heat source, and a right one $t > 0.5$ containing the hyperbolic source. Besides, in Figure 5 right we design another bad

domain decomposition: XPINN-TB, where the domain is partitioned based on the x -axis, because the target function is almost symmetric to $x = 0$, which doesn't split the complexity due to the heterogeneous sources properly.

5.2.2 Results

Table 2 shows the experimental results for the heat equation, and Figure 4 right shows the error distribution of XPINN-LR. The generalization gap, i.e., the testing loss minus the training loss, reveals that XPINN-LR generalizes best, while PINN is the second-best and XPINN-TB is the worst. The theoretical generalization bounds of the three models also point to the same fact, i.e., XPINN-LR performs better than PINN, and PINN performs better than XPINN-TB. Their norms reveal the underlying reason accounting for such performance difference. Specifically, those of XPINN-TB (73.03% and 76.04%) are much closer to that PINN (100%), and are larger than those of XPINN-LR (79.54% and 41.94%) in general, which means XPINN-TB is not a good domain decomposition since the targets in its two subdomains are similar where the complexity is not divided into several simple parts, causing the complexities of sub-nets to not drop enough to compensate for the effect of overfitting due to less data. Moreover, the norms of the two sub-nets in XPINN-TB are similar, which is consistent with our intuition that the target functions in each subdomain are similar.

Furthermore, the norms of XPINN-LR (79.54% and 41.94%) are significantly smaller than that of PINN (100%), especially XPINN-R, which suffices to complement the overfitting impact and leads to better generalization. These facts indicate that appointing different sub-nets to fit each heterogeneous heat source does improve generalization.

5.3 Advection Equation

5.3.1 Setup

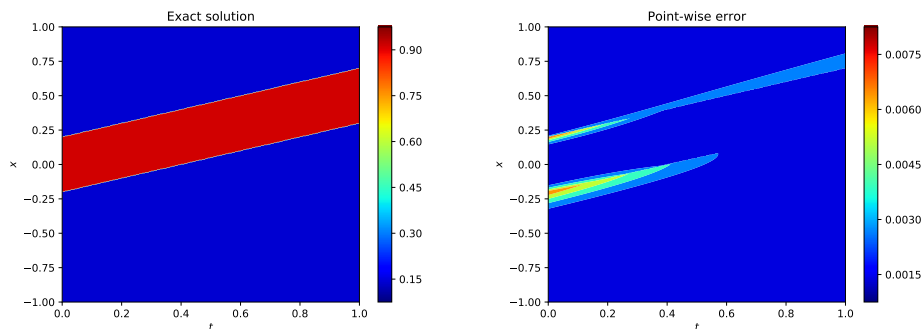


Figure 6: Left: exact solution of the advection equation. Right: error visualization of XPINN-AM.

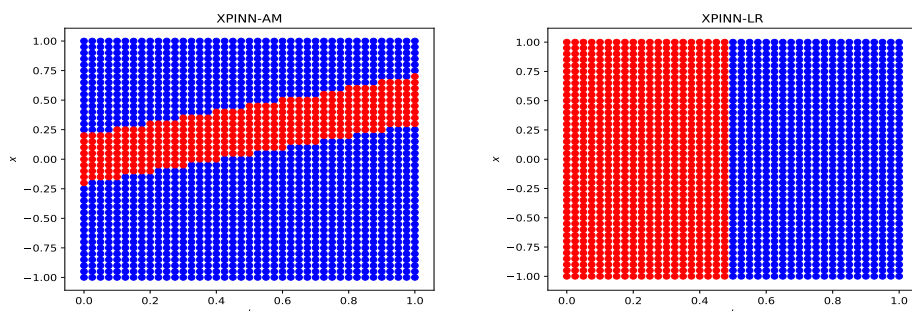


Figure 7: Domain partition in the XPINN of advection equation. Left: XPINN-AM, right: XPINN-LR.

In this subsection, we consider the advection equation to show the difference between XPINN and PINN, which is given by $u_t + 0.5u_x = 0$, $x \in [-1, 1]$, $t \in [0, 1]$, with the initial condition $u(x, 0) = 1_{-0.2 \leq x \leq 0.2}$. The solution is presented in Figure 6 left. The training dataset for PINN contains 10201 residual points and 101 boundary points, whereas the testing dataset for PINN contains 160801 points within the domain. The backbone model for PINN is a 4-layer neural network with 20 hidden units activated by sine as in our theory. Adam [21] optimizer with $1e-3$ learning rate is used for optimization. No regularization is used.

Table 3: Computational results for advection equation.

Method	Train Loss	Test Loss	Norms	Theoretical Bound
PINN	$1.552e-2 \pm 2.824e-3$	$1.652e-2 \pm 3.026e-3$	100.00%	100.00%
XPINN-A	$1.920e-2 \pm 4.101e-3$	$1.586e-2 \pm 2.323e-3$	83.10%	88.20%
XPINN-M			24.03%	
XPINN-L	$1.789e-2 \pm 8.964e-5$	$1.913e-2 \pm 1.043e-4$	68.92%	98.11%
XPINN-R			45.44%	

For XPINN, from Figure 6 left, we observe that the solution of the advection equation can be divided into the following two parts, $\{-0.2 < x - 0.5t\} \cap \{x - 0.5t < 0.2\}$ where $u = 1$ and $\{x - 0.5t \geq 0.2\} \cup \{x - 0.5t \leq -0.2\}$ where $u = 0$. Hence, in XPINN-AM (around and middle), we partition the domain into these two parts mentioned above, which is shown in Figure 7 left. XPINN-AM seems to be a good partition since in each subdomain the target function is extremely simple constant function, while the whole function is complex and discontinuous. In contrast, in XPINN-LR, shown in Figure 7 right, we partition the domain into a left part $\{t \leq 0.5\}$ and a right part $\{t > 0.5\}$, which is problematic because the target functions in each subdomain is not simpler, but discontinuous.

5.3.2 Results

Table 3 presents all computational results for the advection equation, and Figure 6 right shows the error distribution of XPINN-AM. The generalization gap signifies that XPINN-AM generalizes best, while PINN and XPINN-TB are worse than XPINN-AM and they perform similarly. The testing loss of XPINN-AM is even smaller than its training loss. This is not contradictory because the error of XPINN-AM concentrates in small areas near the boundary of domain decomposition (Figure 6 right). Since the testing points are denser than training points, the majority of the former are in areas with smaller errors, rather than near the interface where errors are large, which results in a smaller testing loss.

The reason is revealed by the norms. The norms of XPINN-AM are smaller than PINN, because in each subdomain of XPINN-AM the target function is constant, whose positive influence is more obvious than the overfitting due to less data. At the same time, although norms of XPINN-LR are also smaller than PINN, due to less training data to be fitted and smaller domain, they are still larger than XPINN-AM ($68.92\% + 45.44\%$ (XPINN-LR) $>$ $83.10\% + 24.03\%$ (XPINN-AM)), because the target functions in each subdomain of XPINN-LR are still highly complex discontinuous functions. The decreased complexity in XPINN-LR is not obvious enough to positively affect its generalization.

To conclude, even for the same PDE, the domain decomposition method plays a vital role in generalization. A good XPINN should partition the target function into several simpler pieces to maximize its generalization ability. XPINN-AM partitions it into two extremely simple constant functions, while the decomposition XPINN-LR maintains the complexity of the original target, which causes the variations in their performance.

5.4 Wave Equation

5.4.1 Setup

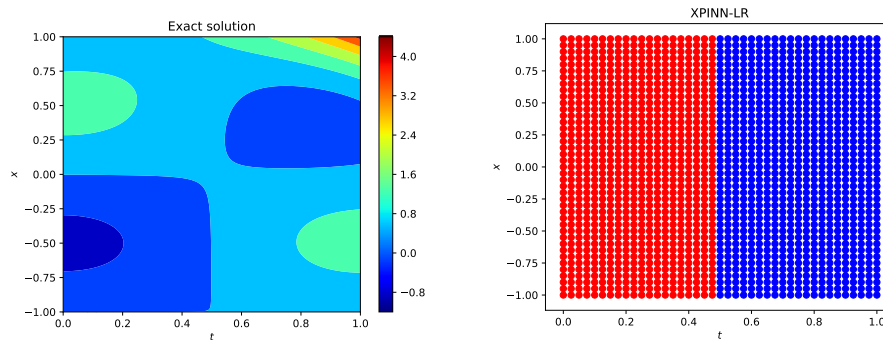


Figure 8: Left: Visualization of the exact solution of wave equation. Right: domain decomposition in XPINN-LR.

In this subsection, we consider the wave equation, which is a second-order linear PDE and is given by $u_{tt} = u_{xx}$, $x \in [-1, 1]$, $t \in [0, 1]$, with the boundary conditions given by the solution $u(x, t) = 0.008e^{\pi x} e^{\pi t} + \sin(\pi x) \cos(\pi t)$. The solution is visualized in Figure 8 left. The training dataset for PINN contained 1681 residual points and 162

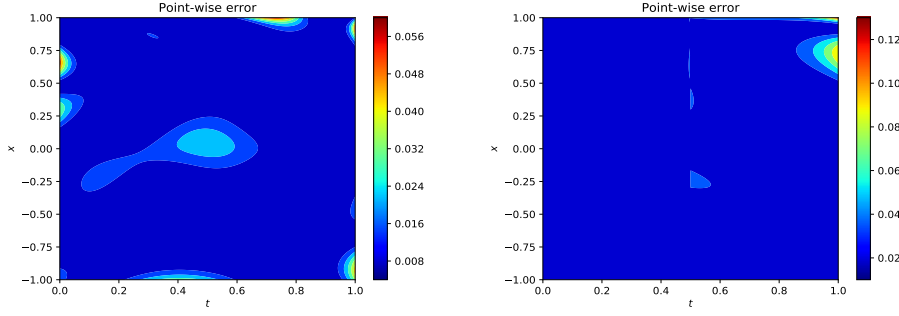


Figure 9: Left: Visualization of error of PINN in wave equation. Right: Visualization of error of XPINN in wave equation.

Table 4: Computational results for wave equation.

Method	Train Loss	Test Loss	Norms	Theoretical Bound
PINN	$1.188e-2 \pm 4.765e-3$	$1.155e-2 \pm 4.959e-3$	100.00%	100.00%
XPINN-L	$1.153e-2 \pm 2.172e-3$	$1.292e-2 \pm 3.684e-3$	59.83%	318.06%
XPINN-R			132.02%	

boundary points, whereas the testing dataset for PINN contains 160801 points within the domain. PINN uses a 6-layer neural network with 32 hidden units activated by sine. Adam [21] optimizer with $1e-3$ learning rate is used. No regularization is used.

For XPINN, from Figure 8 left, we observe that the solution of the wave equation is dominated by the term $\sin(\pi x) \cos(\pi t)$, while the $0.008e^{\pi x} e^{\pi t}$ part is only obvious near $(1, 1)$. We try to design a decomposition method which can split the complexities induced by the two terms into different domains. Specifically, we partition the domain into a left one $t \leq 0.5$ where the term $\sin(\pi x) \cos(\pi t)$ dominates, and a right one $t > 0.5$ where the term $0.008e^{\pi x} e^{\pi t}$ dominates.

5.4.2 Results

The results in Table 4 show that even though both models have similar training loss, the testing performance of XPINN is much worse than PINN, as XPINN has a larger generalization gap, which is also indicated by the theoretical generalization bounds. For the complexities, we observe that sub-net XPINN-L shows significant simplicity compared to PINN, but XPINN-R is extremely complex, even more so than PINN. The former may be due to the fact that the decomposed function in the left subdomain is actually simpler because it does not include the part near $(1, 1)$. The latter may be due to the overfitting caused by fewer available training samples and the extremely complex part near $(1, 1)$ in the right subdomain. The above analysis is also justified by Figure 9, where the error distributions of PINN and XPINN-LR are presented. They reveal that XPINN-L does improve generalization in the left domain where errors are decreased. However, XPINN-R's performance is much worse and the error near $(1, 1)$ is extremely large, which leads to the bad performance of XPINN-LR in general. Although the left subdomain contributes to better generalization, the negative impact of the right subdomain containing the complicated part near $(1, 1)$ is much more obvious.

To conclude, the problems of XPINN are in the subdomain XPINN-R near $(1, 1)$. Because that part changes too drastically and thus is very complex to fit, the less available training data caused by domain decomposition negatively impacts the generalization on this part significantly, which in turn leads to poor overall generalization.

5.5 Compressible Euler Equations

5.5.1 Setup

Next, we consider the nonlinear inviscid compressible Euler equations, which govern the physics of high-speed compressible fluid flows. The inviscid compressible Euler equations admit discontinuous solutions called shock or contact waves, which are difficult to capture with good accuracy. The two-dimensional steady-state Euler equations are given as $F_x(U) + F_y(U) = 0$, $(x, y) \in [0, 1]^2$, where fluxes in x and y directions are defined as $F_x(U) = (\rho u, p + \rho u^2, \rho uv, pu + \rho uE)$ and $F_y(U) = (\rho v, \rho vw, p + \rho v^2, pv + \rho vE)$, where ρ, u, v and p are density, velocity components in x and y directions, and pressure, respectively. The total energy E is defined as $E = \frac{p}{\rho(\gamma-1)} + \frac{1}{2} \|\mathbf{u}\|_2^2$, where $\mathbf{u} = (u, v)$. In this case, we are solving the oblique shock wave problem on a square domain $[0, 1]^2$. The bottom

Table 5: Computational results for compressible Euler equations.

Method	Train Loss	Test Loss	Norms	Theoretical Bound
PINN	$1.819e-3 \pm 6.043e-4$	$2.080e-3 \pm 5.142e-4$	100.00%	100.00%
XPINN-A	$9.210e-4 \pm 1.882e-4$	$1.182e-3 \pm 2.213e-4$	34.44%	91.75%
XPINN-M			72.24%	
XPINN-T	$1.067e-3 \pm 4.829e-4$	$2.083e-3 \pm 2.489e-4$	48.78%	178.21%
XPINN-B			142.57%	

boundary is the wall where slip boundary conditions are applied, whereas left and top boundary are the inflow boundary where Dirichlet boundary conditions are applied. The right boundary has extrapolation boundary conditions. A Mach 2 flow is at an angle of -10 degrees with respect to the bottom wall, which generates an oblique shock at an angle of 29.3 degrees with the bottom horizontal wall. The exact solution is given as

$$(\rho, u, v, p) = \begin{cases} (1.0, \cos 10^\circ, -\sin 10^\circ, 0.17857) & \text{before shock,} \\ (1.4584, 0.8873, 0.0, 0.3047) & \text{after shock.} \end{cases}$$

Among all the primitive variables, we have plotted the fluid density which accurately shows the position of an oblique

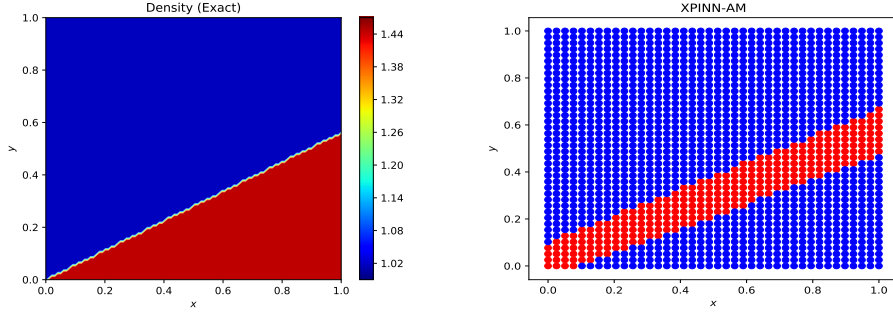


Figure 10: Two-dimensional compressible Euler equations: Exact solution (left) and domain decomposition for XPINN-AM (right).

shock wave. Figure 10 shows the exact value of density (left) and domain decomposition (right) for XPINN-AM. From the domain decomposition figure we observe that the solution of the Euler equations is divided into the following two parts, $\{y \geq 0.57x + 0.1\} \cup \{y \leq 0.5222x - 0.0522\}$, where solution is constant (shown by blue points) and the remaining strip (shown by red points), where oblique shock wave is present.

5.5.2 Results

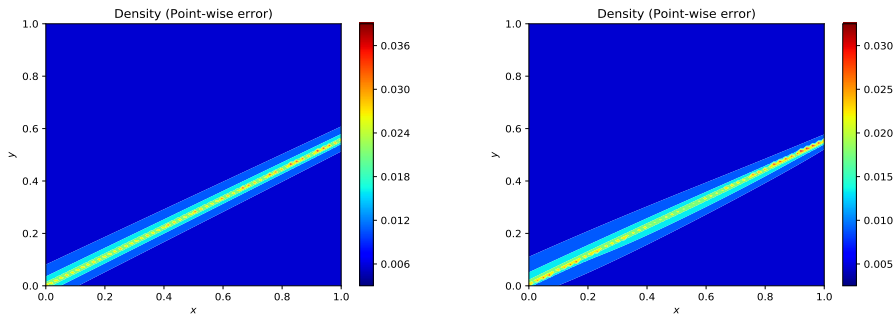


Figure 11: Two-dimensional compressible Euler equations: Point-wise errors for PINN (left) and XPINN (right).

We used a deep net with 10000 residual points, 5 hidden-layers with 20 neurons in each layer, and $8e-4$ learning rate. The activation function is hyperbolic tangent. Table 5 gives the computational results, and Figure 11 gives the point-wise error for the density of the fluid. In this case, the XPINN-AM generalizes better than PINN. Furthermore,

the norms of XPINN-AM (34.44% and 72.24%) are much smaller than that of PINN (100%). We further divide the domain into top ($y \geq 0.5$) and bottom subdomains ($y < 0.5$) for XPINN-TB. The XPINN-TB does not generalize well compared to PINNs, and the complexities of the two sub-nets are 48.78% and 142.57% for top and bottom subdomains, respectively. These results prove that the norms and generalization bounds are good indicators for XPINN based domain decomposition, and can be efficiently used to further decompose the subdomains.

6 Conclusion

In this study, we have investigated the generalization abilities of PINNs and XPINNs, as well as when and how XPINNs improve generalization. For this purpose, we have provided both prior and posterior generalization bounds to explain this from different viewpoints, where for the former we have developed the Barron space for multi-layer networks, while for the latter we have derived the complexity of norm-based Rademacher for PINNs.

Through our discussion on theoretical results, analytical examples, and extensive experiments, we conclude that the domain decomposition method in XPINNs introduces a tradeoff on generalization. On the one hand, its advantage is that it decomposes the complex target function into several simple parts, which lead to the phenomenon that the sum of all parts is smaller than the whole. However, on the other hand, domain decomposition causes less available training data in each subdomain, leading to higher empirical Rademacher complexity and makes models prone to overfitting. When the complexity reduction brought by XPINN exceeds the increased complexity caused by less training data, XPINN outperforms PINN, as in our experiment on KdV equation, heat equation, advection equation, compressible Euler equation and the analytical example in Section 4.1. When the overfitting caused by insufficient data is more dominant than the simplicity due to domain decomposition, PINN outperforms XPINN, as in our experiment on heat equation, wave equation and our analytical example in Section 4.2. When the two factors reach a balance, XPINN and PINN perform similarly, as shown in our experiment on advection equation and our analytical example in Section 4.3.

Our results can also provide a partial explanation for the following observation. For long-time integration of several PDEs, it has been empirically observed that only XPINNs are applicable as PINNs tend to be inaccurate. According to our theory, this is expected as we tend to have a very high complexity measured by the norms for a whole solution of a long-time integration, which can be decomposed into less complex sub-solutions in XPINNs. Overall, the present work provides the first theoretical understanding on when and how to employ XPINN for better generalization performances over the vanilla PINNs.

Acknowledgment

A. D. Jagtap and G. E. Karniadakis would like to acknowledge the funding by OSD/AFOSR MURI Grant FA9550-20-1-0358, and the US Department of Energy (DOE) PhILMs project (DE-SC0019453).

A Proofs of the Barron Space

A.1 Proof of Theorem 2.2

Proof. (Proof of Theorem 2.2) Because X embeds continuously into $C^{0,1}(\Omega)$, there exists constants $C_1, C_2 > 0$ such that

$$\|g\|_{C^0(\Omega)} \leq C_1 \|g\|_X, [g]_{C^{0,1}(\Omega)} \leq C_2 \|g\|_X, \forall g \in X. \quad (19)$$

Banach Space. By construction, $\mathcal{B}_{X,\Omega}$ is isometric to the quotient space $\mathcal{M}(B^X)/N_K$ where

$$N_K = \left\{ \mu \in \mathcal{M}(B^X) \mid \int_{B^X} \rho(g(\mathbf{x})) d\mu(g) = 0, \forall \mathbf{x} \in \Omega \right\}. \quad (20)$$

In Particular, $\mathcal{B}_{X,\Omega}$ is a normed vector space with the norm $\|\cdot\|_{X,\Omega}$. The map

$$\mathcal{M}(B^X) \rightarrow C^0(\Omega), \mu \rightarrow f_\mu = \int_{B^X} \rho(g) d(\mu(g)), \quad (21)$$

is continuous because

$$\begin{aligned} \left\| \int_{B^X} \rho(g) d(\mu(g)) \right\|_{C^0(\Omega)} &\leq \int_{B^X} \|\rho(g)\|_{C^0(\Omega)} d(|\mu|(g)) \\ &\leq \int_{B^X} \|g\|_{C^0(\Omega)} d(|\mu|(g)) \\ &\leq C_1 \|\mu\|_{\mathcal{M}(B^X)} \end{aligned} \quad (22)$$

by the definition of Brochner integrals. Due to the continuity, N_K is the kernel of a continuous linear map. Therefore, N_K is a closed subspace of \mathcal{M}_{B^X} . By the theorem in functional analysis, we conclude that $\mathcal{B}_{X,\Omega}$ is a Banach space.

$\mathcal{B}_{X,\Omega}$ embeds continuously into $C^{0,1}(\Omega)$. In the proof of statement (1), we already have $\|f_\mu\|_{C^0(\Omega)} \leq C_1 \|\mu\|_{\mathcal{M}(B^X)}$. By taking infimum over μ , we have $\|f\|_{C^0(\Omega)} \leq C_1 \|f\|_{\mathcal{B}_{X,\Omega}}$. Furthermore, for any $\mathbf{x} \neq \mathbf{y} \in \Omega$, we have

$$\begin{aligned} |f_\mu(\mathbf{x}) - f_\mu(\mathbf{y})| &\leq \int_{B^X} |\rho(g(\mathbf{x})) - \rho(g(\mathbf{y}))| d|\mu|(g) \\ &\leq \int_{B^X} |g(\mathbf{x}) - g(\mathbf{y})| d|\mu|(g) \\ &\leq \int_{B^X} [g]_{C^{0,1}(\Omega)} |\mathbf{x} - \mathbf{y}| d|\mu|(g) \\ &\leq C_2 \|\mu\|_{\mathcal{M}(B^X)} |\mathbf{x} - \mathbf{y}| \end{aligned} \quad (23)$$

After taking infimum over μ , we come to the conclusion.

The closed unit ball of $\mathcal{B}_{X,\Omega}$ is a closed subset of $C^0(\Omega)$. We assume that $(f_n)_{n \in \mathbb{N}}$ is a sequence such that $\|f_n\|_{X,K} \leq 1$. Choose a sequence of measures $(\mu_n)_{n \in \mathbb{N}}$ such that $f_n = f_{\mu_n}$ and $\|\mu_n\| \leq 1 + \frac{1}{n}$. These measures exist because f_n are from the unit ball of $\mathcal{B}(X, \Omega)$. By the compactness theorem of Radon measures, there exists a subsequence μ_{n_k} and a Radon measure μ , such that μ_{n_k} weak converge to μ with $\|\mu\| \leq 1$. Since all functions $\rho(g)$ are continuous and bounded, we have $f_{n_k} \rightarrow f_\mu$ in the product topology. In particular, if $f_{\mu_n} \rightarrow \hat{f}$ uniformly, then $\hat{f} = f_\mu \in B^{\mathcal{B}_{X,\Omega}}$, i.e. the unit ball of $\mathcal{B}_{X,\Omega}$ is closed in the $C^0(\Omega)$ topology. \square

A.2 Proof of Theorem A.1

Theorem A.1. (Rademacher Complexity of Generalized Barron Functions). Denote by \mathcal{F} the unit ball of $\mathcal{B}_{X,\Omega}$. Let S be any sample set in Ω . Then

$$\text{Rad}(\mathcal{F}; S) \leq 2\text{Rad}(B^X; S). \quad (24)$$

Proof. (Proof of Theorem A.1) Define the function classes $\mathcal{H}_1 = \{\rho(g) : g \in B^X\}$, $\mathcal{H}_2 = \{-\rho(g) : g \in B^X\}$ and $\mathcal{H} = \mathcal{H}_1 \cup \mathcal{H}_2$. Because ρ is 1-Lipschitz continuous, all the three classes are equicontinuous and closed, and thus precompact, ultimately compact subsets.

We decompose $\mu = \mu^+ - \mu^-$ in its mutually singular positive and negative parts and write $f = f_\mu$ in $\mathcal{B}_{X,\Omega}$ as

$$\begin{aligned} f_\mu(\mathbf{x}) &= \int_{B^X} \rho(g(\mathbf{x})) d\mu^+(g) + \int_{B^X} -\rho(g(\mathbf{x})) d\mu^-(g) \\ &= \int_{\mathcal{H}_1} h(\mathbf{x}) d\rho_{\#}^+ \mu^+(h) + \int_{\mathcal{H}_2} h(\mathbf{x}) d\rho_{\#}^- \mu^-(h) \\ &= \int_{\mathcal{H}} h(\mathbf{x}) d\hat{\mu}(h), \end{aligned} \quad (25)$$

where $\rho: B^X \rightarrow \mathcal{H}$ is given by $g \rightarrow \rho(g)$ and $\hat{\mu} = \rho_{\#}^+ \mu^+ + \rho_{\#}^- \mu^-$. In particular, we note that $\hat{\mu}$ is a non-negative measure and $\|\mu\|_{\mathcal{M}(B^X)} = \|\hat{\mu}\|_{\mathcal{M}(\mathcal{F})}$. We conclude that \mathcal{F} is the closed convex hull of \mathcal{H} .

Since we assume the non-linearity ρ is 1-Lipschitz continuous, the contraction Lemma implies that

$$\begin{aligned} \text{Rad}(\mathcal{F}; S) &= \text{Rad}(\mathcal{H}; S) \\ &= \text{Rad}(\mathcal{H}_1 \cup -\mathcal{H}_1; S) \\ &\leq \text{Rad}(\mathcal{H}_1; S) + \text{Rad}(-\mathcal{H}_1; S) \\ &= 2\text{Rad}(\mathcal{H}_1; S) \\ &= 2\text{Rad}(B^X; S) \end{aligned} \tag{26}$$

since for all ξ , the supremum is non-negative. \square

A.3 Proof of Theorem 2.1

Lemma A.1. *Let \mathcal{G} be a set in a Hilbert space H such that $\|g\|_H \leq R$ for all $g \in \mathcal{G}$. If f is in the closed convex hull of \mathcal{G} , then for every $m \in \mathbb{N}$ and $\epsilon > 0$, there exist m elements $g_1, \dots, g_m \in \mathcal{G}$ such that*

$$\left\| f - \frac{1}{m} \sum_{i=1}^m g_i \right\|_H \leq \frac{R + \epsilon}{\sqrt{m}}. \tag{27}$$

Proof. This lemma is proved by using the law of large numbers. See [22] for details. \square

Proof. (Proof of Theorem 2.1). This is immediate by the definition of generalized Barron space and that of neural networks in Definition 2.1. \square

A.4 Proof of Theorem 2.3

Proof. (Proof of Theorem 2.3) Due to the choice of \mathcal{W}^0 as linear functions, the constants of continuous embedding are $C_1, C_2 = 1$. By the fact that $C^{0,1}(\Omega)$ embeds continuously into L^2 , we have $\|f\|_{L^2} \leq 2\|f\|_{\mathcal{W}^L}$.

Recall that the unit ball of \mathcal{W}^L is the closed convex hull of the class $\mathcal{H} = \{\sigma(g) : \|g\|_{\mathcal{W}^L} = 1\}$. Thus by Lemma, there exists $g_1, \dots, g_m \in \mathcal{W}^{L-1}$ and $\epsilon_1, \dots, \epsilon_m \in \{-1, 1\}$ such that

$$\left\| f - \frac{1}{m} \sum_{i=1}^m \epsilon_i \sigma(g_i(\mathbf{x})) \right\|_{L^2} \leq \frac{3\|f\|_{\mathcal{W}^L}}{\sqrt{m}}. \tag{28}$$

If $L = 1$, g_i are linear functions and $u_m(\mathbf{x}) = \sum_{i=1}^m \frac{\epsilon_i}{m} \sigma(g_i(\mathbf{x}))$ is a two-layer neural network. Thus the case $L = 1$ in the theorem is proved.

We prove the remain by induction. Assume that the theorem has been proved for the case of $L - 1$. Then we note that $\|g_i\|_{\mathcal{W}^L} = 1$, so for $1 \leq i \leq m$ we can find a finite $L - 1$ -layer network \hat{g}_i such that

$$\begin{aligned} \left\| f - \frac{1}{m} \epsilon_i \sigma(\hat{g}_i(\mathbf{x})) \right\|_{L^2} &\leq \left\| f - \frac{1}{m} \epsilon_i \sigma(g_i(\mathbf{x})) \right\|_{L^2} + \frac{1}{m} \sum_{i=1}^m \|g_i - \hat{g}_i\|_{L^2} \\ &\leq \frac{3}{\sqrt{m}} + \frac{m \cdot 3(L-1)}{m \sqrt{m}} \\ &= \frac{3L}{\sqrt{m}}. \end{aligned} \tag{29}$$

We merge the m trees associated with \hat{g}_i into a single tree, increasing the width of each layer by a factor of m , and add an outer layer of width m with coefficients W . \square

B Proofs of Rademacher Complexity

In this section, we provide proofs for Rademacher complexity. We begin by several well-known useful results.

Lemma B.1. *(Rademacher Complexity of Linear Functions). If \mathcal{H}_{lin} is the class of linear functions on \mathbb{R}^d with l^1 -norm smaller or equal to 1 and S is any sample set of n elements in Ω , then*

$$\text{Rad}(\mathcal{H}_{lin}; S) \leq \sqrt{\frac{2 \log(2d)}{n}}. \tag{30}$$

Lemma B.2. (Contraction lemma). Suppose that $\phi_i : \mathbb{R} \rightarrow \mathbb{R}$ is a C_L -Lipschitz function for each $i \in \{1, 2, \dots, n\}$. For any $\mathbf{y} \in \mathbb{R}^n$, let $\phi(\mathbf{y}) = (\phi_1(y_1), \phi_2(y_2), \dots, \phi_n(y_n))^T$. For an arbitrary set of vector functions \mathcal{F} of length n on an arbitrary domain \mathcal{Z} and an arbitrary choice of samples $S = \{\mathbf{z}_1, \mathbf{z}_2, \dots, \mathbf{z}_n\} \subset \mathcal{Z}$, we have

$$\text{Rad}(\phi \circ \mathcal{F}; S) \leq C_L \text{Rad}(\mathcal{F}; S). \quad (31)$$

Based on the above lemma, we are in a position to prove a key lemma frequently used in Rademacher complexity of PINNs.

Lemma B.3. Let \mathcal{F} be an arbitrary function class on \mathbb{R}^d , and $|f(\mathbf{x})| \leq M$ be a bounded function. Then for arbitrary choice of samples $S = \{\mathbf{x}_1, \mathbf{x}_2, \dots, \mathbf{x}_n\}$, the Rademacher complexity of the function class $f(\mathbf{x}) \cdot \mathcal{F}$ satisfies

$$\text{Rad}(f(\mathbf{x}) \cdot \mathcal{F}; S) \leq M \text{Rad}(\mathcal{F}; S) \quad (32)$$

Proof. Apply the previous lemma with $\phi_i(y_i) = f(\mathbf{x}_i)y_i$ for all i , whose Lipschitz constant is at most M . \square

After that, we provide full details for the second order derivatives of neural networks.

$$\begin{aligned} & \frac{\partial^2 u_{\theta}(\mathbf{x})}{\partial \mathbf{x}^2} \\ & \stackrel{(1)}{=} \frac{\partial \text{vec}(\mathbf{W}^L \cdot \Phi^{L-1} \mathbf{W}^{L-1} \dots \Phi^1 \mathbf{W}^1)}{\partial \mathbf{x}} \\ & \stackrel{(2)}{=} \sum_{l=1}^{L-1} \frac{\partial \text{vec}(\mathbf{W}^L \cdot \Phi^{L-1} \mathbf{W}^{L-1} \dots \Phi^1 \mathbf{W}^1)}{\partial \text{vec}(\Phi^l)} \frac{\partial \text{vec}(\Phi^l)}{\partial \mathbf{x}}, \\ & \stackrel{(3)}{=} \sum_{l=1}^{L-1} (\mathbf{W}^l \dots \Phi^1 \mathbf{W}^1)^T \otimes (\mathbf{W}^L \Phi^{L-1} \dots \mathbf{W}^{l+1}) \frac{\partial \text{vec}(\Phi^l)}{\partial \mathbf{x}} \\ & \stackrel{(4)}{=} \left\{ \sum_{l=1}^{L-1} (\mathbf{W}^l \dots \Phi^1 \mathbf{W}^1)^T \otimes (\mathbf{W}^L \Phi^{L-1} \dots \mathbf{W}^{l+1}) \frac{\partial \text{vec}(\Phi^l)}{\partial \mathbf{x}_j} \right\}_{1 \leq j \leq d} \\ & = \left\{ \sum_{l=1}^{L-1} (\mathbf{W}^l \dots \Phi^1 \mathbf{W}^1)^T \otimes (\mathbf{W}^L \Phi^{L-1} \dots \mathbf{W}^{l+1}) \frac{\partial \text{vec}(\text{diag}[\sigma'(\mathbf{W}^l \sigma(\dots \mathbf{W}^1 \mathbf{x}))])}{\partial \mathbf{x}_j} \right\}_{1 \leq j \leq d} \\ & = \left\{ \sum_{l=1}^{L-1} (\mathbf{W}^l \dots \Phi^1 \mathbf{W}^1)^T \otimes (\mathbf{W}^L \Phi^{L-1} \dots \mathbf{W}^{l+1}) \text{vec}(\text{diag}[\frac{\partial \sigma'(\mathbf{W}^l \sigma(\dots \mathbf{W}^1 \mathbf{x}))}{\partial \mathbf{x}_j}]) \right\}_{1 \leq j \leq d} \\ & = \left\{ \sum_{l=1}^{L-1} (\mathbf{W}^l \dots \Phi^1 \mathbf{W}^1)^T \otimes (\mathbf{W}^L \Phi^{L-1} \dots \mathbf{W}^{l+1}) \text{vec}(\text{diag}[\Psi^l \mathbf{W}^l \dots \Psi^1 \mathbf{W}^1_{:,j}]) \right\}_{1 \leq j \leq d} \\ & \stackrel{(5)}{=} \left\{ \sum_{l=1}^{L-1} (\mathbf{W}^L \Phi^{L-1} \dots \mathbf{W}^{l+1}) \text{diag}(\Psi^l \mathbf{W}^l \dots \Psi^1 \mathbf{W}^1_{:,j}) (\mathbf{W}^l \dots \Phi^1 \mathbf{W}^1) \right\}_{1 \leq j \leq d}. \end{aligned} \quad (33)$$

In (1), note that $\text{vec}(\mathbf{W}^L \cdot \Phi^{L-1} \mathbf{W}^{L-1} \dots \Phi^1 \mathbf{W}^1) \in \mathbb{R}^d$, $\mathbf{x} \in \mathbb{R}^d$, thus the result of (1) is in $\mathbb{R}^{d \times d}$. In (2), we apply the chain rule, with the first term $\in \mathbb{R}^{d \times m_l^2}$ and the second term $\in \mathbb{R}^{m_l^2 \times d}$. In (3) we use the formula $\frac{\partial \text{vec}(AXB)}{\partial \text{vec}(X)} = B^T \otimes A$, and the first term $\in \mathbb{R}^{d \times m_l}$, second $\in \mathbb{R}^{1 \times m_l}$, third $\in \mathbb{R}^{m_l^2 \times d}$. In (4), we decompose the calculation into dimensional-wise with $\frac{\partial \text{vec}(\Phi^l)}{\partial \mathbf{x}_j} \in \mathbb{R}^{m_l^2}$. In (5), we use the fact that $B^T \otimes \text{Avec}(X) = \text{vec}(AXB)$.

B.1 Tree-Like Function Space

Lemma B.4. Suppose $\mathbf{W}^l \in \mathbb{R}^{m_l \times m_{l-1}}$, $1 \leq l \leq L$ are a sequence of matrices whose rows are l^1 normalized, i.e. $\|\mathbf{W}^l\|_{1,\infty} \leq 1$, $\forall 1 \leq l \leq L$. Then all rows of $\mathbf{W} = \mathbf{W}^L \cdot \mathbf{W}^{L-1} \dots \mathbf{W}^1$ are also l^1 normalized, i.e. $\|\mathbf{W}\|_{1,\infty} \leq 1$.

Proof. By induction, we only need to proof the case when $L = 2$. Note that the i -th row of $\mathbf{W}^2\mathbf{W}^1$ satisfies

$$\begin{aligned} \|[\mathbf{W}^2\mathbf{W}^1]_i\|_1 &\leq \sum_{j=1}^n |\mathbf{W}_{ij}^2| \|\mathbf{W}_j^1\|_1 \\ &\leq \sum_{j=1}^n |\mathbf{W}_{ij}^2| \\ &\leq 1. \end{aligned} \quad (34)$$

□

Lemma B.5. (*Rademacher Complexity of Tree-Like Functions*). For every L , and every set of n points $S \subset \Omega$, the hypothesis class \mathcal{H}^L given by the closed unit ball in \mathcal{W}^L satisfies the Rademacher complexity bound

$$\text{Rad}(\mathcal{H}^L; S) \leq 2^L \sqrt{\frac{2 \log(2d)}{n}}. \quad (35)$$

Proof. Recursively apply Theorem A.1 and the above lemma of Rademacher complexity of linear functions. □

Remark. The Rademacher complexity for tree-like functions is very general which applies to all tree-like functions and thus it is too pessimistic for special types of tree-like functions such as neural networks. Hence, in the next two subsections, we improve the Rademacher complexity for neural networks, based on the approaches in [23] and [24] respectively.

B.2 One-Infinity Norm for Complexity

We need first a technical lemma, which is key to avoid exponential dependency on the network depth.

Lemma B.6. (*Lemma 2 in [23]*). Let σ be a 1-Lipschitz activation function with $\sigma(0) = 0$, applied element-wise. Then for any vector-valued class \mathcal{F} , and any convex and monotonically increasing function $g : \mathbb{R} \rightarrow [0, \infty)$,

$$\mathbb{E}_\epsilon \sup_{f \in \mathcal{F}, \|\mathbf{W}\|_{1, \infty} \leq Q} g\left(\left\|\sum_{i=1}^n \epsilon_i \sigma(\mathbf{W}f(\mathbf{x}_i))\right\|_\infty\right) \leq 2 \cdot \mathbb{E}_\epsilon \sup_{f \in \mathcal{F}} g\left(Q \cdot \left\|\sum_{i=1}^n \epsilon_i f(\mathbf{x}_i)\right\|_\infty\right). \quad (36)$$

Proof. Note that the sine activation function used in this paper satisfies the assumptions in this lemma. For the detailed proof readers are referred to the proof of Lemma 2 in [23]. □

Lemma B.7. (*$(1, \infty)$ Norm Controlled Rademacher Complexity of Neural Networks*). For every L , and every set of n points $S \subset \Omega$, the hypothesis class \mathcal{NN}_M^L given by the neural networks

$$\mathcal{NN}_M^L = \left\{ u_\theta(\mathbf{x}) = \mathbf{W}^L \sigma(\mathbf{W}^{L-1} \sigma(\dots \sigma(\mathbf{W}^1 \mathbf{x}))) \mid \|\mathbf{W}^l\|_{1, \infty} \leq M(l), \forall l \right\}, \quad (37)$$

satisfies the Rademacher complexity bound

$$\text{Rad}(\mathcal{NN}_M^L; S) \leq 2 \prod_{l=1}^L M(l) \sqrt{\frac{L+1+\log(d)}{n}}. \quad (38)$$

Proof. To be self-contained, we prove this crucial lemma, which is similar to the proof of Theorem 2 in [23].

We begin with several new notations to simplify the proof. We let \mathbf{W}_b^r be shorthand for the matrix tuple $\{\mathbf{W}^r, \mathbf{W}^{r-1}, \dots, \mathbf{W}^b\}$, and \mathcal{N}_b^r denote the function computed by the sub-network composed of layers b through r , that is

$$x \rightarrow \mathbf{W}^r \sigma(\mathbf{W}^{r-1} \sigma(\dots \sigma(\mathbf{W}^b \mathbf{x}))). \quad (39)$$

We fix constant $\lambda > 0$ to be chosen later, the Rademacher complexity can be upper bounded as

$$\begin{aligned} n\text{Rad}(\mathcal{NN}_M^L; S) &= \mathbb{E}_\epsilon \sup_{\mathbf{N}_1^{L-1}, \mathbf{W}^L} \sum_{i=1}^n \epsilon_i \mathbf{W}^L \sigma(\mathcal{N}_1^{L-1}(\mathbf{x}_i)) \\ &\leq \frac{1}{\lambda} \log \mathbb{E}_\epsilon \sup \exp\left(\lambda \sum_{i=1}^n \epsilon_i \mathbf{W}^L \sigma(\mathcal{N}_1^{L-1}(\mathbf{x}_i))\right) \\ &\leq \frac{1}{\lambda} \log \mathbb{E}_\epsilon \sup \exp\left\{M(L) \cdot \left\|\sum_{i=1}^n \lambda \epsilon_i \sigma(\mathcal{N}_1^{L-1}(\mathbf{x}_i))\right\|_\infty\right\}. \end{aligned} \quad (40)$$

Recursively apply the above deduction from $L, L-1$ to 1, and applying Lemma B.6, we can upper bound the above by

$$n\text{Rad}(\mathcal{N}\mathcal{N}_M^L; S) \leq \frac{1}{\lambda} \log(2^L \cdot \mathbb{E}_\epsilon \exp(M\lambda \|\sum_{i=1}^n \epsilon_i \mathbf{x}_i\|_\infty)), \quad (41)$$

where $M = \prod_{l=1}^L M(l)$. Furthermore, using symmetry, the expectation inside the log can be rewritten as

$$\begin{aligned} \mathbb{E}_\epsilon \exp(M\lambda \cdot \max_j |\sum_{i=1}^n \epsilon_i x_{i,j}|) &\leq \sum_{j=1}^d \mathbb{E}_\epsilon \exp(M\lambda \cdot |\sum_{i=1}^n \epsilon_i x_{i,j}|) \\ &\leq \sum_{j=1}^d \mathbb{E}_\epsilon [\exp(M\lambda \cdot \sum_{i=1}^n \epsilon_i x_{i,j}) + \exp(-M\lambda \cdot \sum_{i=1}^n \epsilon_i x_{i,j})] \\ &= 2 \sum_{j=1}^d \mathbb{E}_\epsilon \exp(M\lambda \cdot \sum_{i=1}^n \epsilon_i x_{i,j}) \\ &= 2 \sum_{j=1}^d \prod_{i=1}^n \mathbb{E}_\epsilon \exp(M\lambda \epsilon_i x_{i,j}) \\ &= \sum_{j=1}^d \prod_{i=1}^n [\exp(M\lambda x_{i,j}) + \exp(-M\lambda x_{i,j})] \\ &= 2 \sum_{j=1}^d \exp(M^2 \lambda^2 \sum_{i=1}^n x_{i,j}^2), \end{aligned} \quad (42)$$

where in the last step we used the fact that $\frac{\exp(z) + \exp(-z)}{2} \leq \exp(z^2/2)$.

Further upper bounding this by $2d \max_j \exp(M^2 \lambda^2 \sum_{i=1}^n x_{i,j}^2)$ and pluggin back to equation (41), we get

$$\frac{1}{\lambda} \log(2^{L+1} d \cdot \max_j \exp(M^2 \lambda^2 \sum_{i=1}^n x_{i,j}^2)) = \frac{L+1+\log(d)}{\lambda} + M^2 \lambda \max_j \sum_{i=1}^n x_{i,j}^2. \quad (43)$$

Choosing $\lambda = \sqrt{\frac{L+1+\log(d)}{M^2 \max_j \sum_{i=1}^n x_{i,j}^2}}$, we can upper bound the above by

$$2M \sqrt{n(L+1+\log(d))} \quad (44)$$

because $\mathbf{x}_{i,j} \in [0, 1]$. \square

Remark. This key lemma indicates the Rademacher complexity of neural networks in Definition 2.1 is directly controlled by their path norms, which are associated with their Barron norms. This is because for DNNs in Definition 2.1, we have $\|\mathbf{W}^l\|_{1,\infty} \leq 1, \forall l < L$ and $\prod_{l=1}^L M(l) = \prod_{l=1}^L \|\mathbf{W}^l\|_{1,\infty} \leq \|\mathbf{W}^L\|_{1,\infty} = \|\boldsymbol{\theta}\|_{\mathcal{P}}$. We thus bridge Rademacher complexity with Barron space.

Lemma B.8. (*1, ∞ Norm Controlled Rademacher Complexity of Differentiated Networks*). For every L , and every set of n points $S \subset \bar{\Omega}$, the hypothesis class $\mathcal{P}\mathcal{I}\mathcal{N}\mathcal{N}_M^L$ given by

$$\mathcal{P}\mathcal{I}\mathcal{N}\mathcal{N}_M^L = \{\mathcal{L}u \mid u \in \mathcal{N}\mathcal{N}_M^L\}, \quad (45)$$

satisfies the Rademacher complexity bound

$$\text{Rad}(\mathcal{P}\mathcal{I}\mathcal{N}\mathcal{N}_M^L; S) \leq 2M[1 + M(1) + d(L-1)M(1)^2] \prod_{l=1}^L M(l) \sqrt{\frac{L+1+\log(d)}{n}}. \quad (46)$$

Proof. We first have

$$\mathcal{P}\mathcal{I}\mathcal{N}\mathcal{N}_M^L = \{f(\mathbf{x}) \mid f(\mathbf{x}) = f_1(\mathbf{x}) + f_2(\mathbf{x}) + f_3(\mathbf{x})\}, \quad (47)$$

where

$$\begin{aligned} f_1(\mathbf{x}) &= \sum_{\alpha=1, \beta=1}^d A_{\alpha\beta}(\mathbf{x}) u_{x_\alpha x_\beta}(\mathbf{x}), \\ f_2(\mathbf{x}) &= \mathbf{W}^L \cdot \boldsymbol{\Phi}^{L-1} \mathbf{W}^{L-1} \dots \boldsymbol{\Phi}^1 \mathbf{W}^1 \mathbf{b}(\mathbf{x}), \\ f_3(\mathbf{x}) &= c(\mathbf{x}) \mathbf{W}^L \sigma(\mathbf{W}^{L-1} \sigma(\dots \sigma(\mathbf{W}^1 \mathbf{x}))). \end{aligned} \quad (48)$$

Thus

$$\mathcal{PINN}_M^L \subset \mathcal{F}_1 + \mathcal{F}_2 + \mathcal{F}_3, \quad (49)$$

where

$$\begin{aligned} \mathcal{F}_1 &= \left\{ f_1(\mathbf{x}) \mid f_1(\mathbf{x}) = \sum_{\alpha=1, \beta=1}^d A_{\alpha\beta}(\mathbf{x}) u_{x_\alpha x_\beta}(\mathbf{x}), \text{ where } u(\mathbf{x}) \in \mathcal{NN}_M^L \right\}, \\ \mathcal{F}_2 &= \left\{ f_2(\mathbf{x}) \mid f_2(\mathbf{x}) = \mathbf{W}^L \cdot \Phi^{L-1} \mathbf{W}^{L-1} \dots \Phi^1 \mathbf{W}^1 \mathbf{b}(\mathbf{x}), \text{ where } u \in \mathcal{NN}_M^L \right\}, \\ \mathcal{F}_3 &= c(\mathbf{x}) \mathcal{NN}_M^L. \end{aligned} \quad (50)$$

We first consider the simplest function class \mathcal{F}_3 . Its Rademacher complexity can be derived directly using Lemma B.2

$$\begin{aligned} \text{Rad}(\mathcal{F}_3; S) &\leq M \text{Rad}(\mathcal{NN}_M^L; S) \\ &\leq 2K \prod_{l=1}^L M(l) \sqrt{\frac{L+1+\log(d)}{n}}. \end{aligned} \quad (51)$$

However, tackling \mathcal{F}_2 and \mathcal{F}_1 are much more complicated, we proceed by the proof for \mathcal{F}_2 , by definition we have

$$\begin{aligned} n \text{Rad}(\mathcal{F}_2; S) &= \mathbb{E}_\epsilon \sup_{\boldsymbol{\theta}} \sum_{i=1}^n \mathbf{W}^L \dots \Phi^1 \mathbf{W}^1 \mathbf{b}(\mathbf{x}_i) \epsilon_i \\ &\leq \mathbb{E}_\epsilon \sup_{\boldsymbol{\theta}} \left| \sum_{i=1}^n \mathbf{W}^L \dots \mathbf{W}^2 \Phi^1 \epsilon_i \mathbf{W}^1 \mathbf{b}(\mathbf{x}_i) \right| \\ &= \mathbb{E}_\epsilon \sup_{\boldsymbol{\theta}} \left| \mathbf{W}^L \sum_{i=1}^n \Phi^{L-1}(\mathbf{x}_i) \dots \mathbf{W}^2 \Phi^1(\mathbf{x}_i) \epsilon_i \mathbf{W}^1 \mathbf{b}(\mathbf{x}_i) \right| \\ &\stackrel{(1)}{\leq} M(L) \mathbb{E}_\epsilon \sup_{\boldsymbol{\theta}} \left\| \sum_{i=1}^n \Phi^{L-1}(\mathbf{x}_i) \dots \mathbf{W}^2 \Phi^1(\mathbf{x}_i) \epsilon_i \mathbf{W}^1 \mathbf{b}(\mathbf{x}_i) \right\|_\infty, \end{aligned} \quad (52)$$

where (1) is due to Holder inequality. Since $\Phi(\mathbf{x}_i)$ depends on the samples, we cannot directly perform peeling just like what we have already done for \mathbf{W}^L . We also need to avoid the exponential dependency on depth due to the peeling of $\|\cdot\|_\infty$. We first notice that in the above equation, only the first two terms $\Phi^{L-1}(\mathbf{x}_i) \mathbf{W}^{L-1}$ depend on the $(L-1)$ -th layer parameters \mathbf{W}^{L-1} . Moreover, if we view $\Phi^{L-1}(\mathbf{x}_i) \mathbf{W}^{L-1}$ as a whole, it becomes a matrix whose i -th row only depends on the i -th row of \mathbf{W}^{L-1} . Hence, we only need to consider \mathbf{W}^{L-1} as a vector since all of its rows are equivalent. For any convex and monotonically increasing function $g: \mathbb{R} \rightarrow [0, \infty)$

$$\begin{aligned} &\mathbb{E}_\epsilon \sup g \left(\left\| \sum_{i=1}^n \Phi^{L-1}(\mathbf{x}_i) \dots \mathbf{W}^2 \Phi^1(\mathbf{x}_i) \epsilon_i \mathbf{W}^1 \mathbf{b}(\mathbf{x}_i) \right\|_\infty \right) \\ &= \mathbb{E}_\epsilon \sup_{\mathbf{W}^{L-1} \in \mathbb{R}^{m_{L-1}}} g \left(\left| \sum_{i=1}^n \sigma'(\mathbf{W}^{L-1} \sigma(\dots \mathbf{x}_i)) \mathbf{W}^{L-1} \dots \mathbf{W}^2 \Phi^1(\mathbf{x}_i) \epsilon_i \mathbf{W}^1 \mathbf{b}(\mathbf{x}_i) \right| \right) \\ &= \mathbb{E}_\epsilon \sup_{\mathbf{W}^{L-1} \in \mathbb{R}^{m_{L-1}}} g(|z|) \\ &\leq \mathbb{E}_\epsilon \sup_{\mathbf{W}^{L-1} \in \mathbb{R}^{m_{L-1}}} g(z) + g(-z) \\ &\leq 2 \mathbb{E}_\epsilon \sup_{\mathbf{W}^{L-1} \in \mathbb{R}^{m_{L-1}}} g(z) \\ &= 2 \mathbb{E}_\epsilon \sup_{\mathbf{W}^{L-1} \in \mathbb{R}^{m_{L-1}}} g \left(\sum_{i=1}^n \sigma'(\mathbf{W}^{L-1} \sigma(\dots \mathbf{x}_i)) \mathbf{W}^{L-1} \dots \mathbf{W}^2 \Phi^1(\mathbf{x}_i) \epsilon_i \mathbf{W}^1 \mathbf{b}(\mathbf{x}_i) \right), \end{aligned} \quad (53)$$

where we have used the fact that $g(|z|) \leq g(z) + g(-z)$ and temporarily denoted $z = \sum_{i=1}^n \sigma'(\mathbf{W}^{L-1} \sigma(\dots \mathbf{x}_i)) \mathbf{W}^{L-1} \dots \mathbf{W}^2 \Phi^1(\mathbf{x}_i) \epsilon_i \mathbf{W}^1 \mathbf{b}(\mathbf{x}_i)$. And in $g(-z)$ the $-$ can be absorbed into the Rademacher random variables ϵ_i without changing the distribution of all ϵ .

We are now in a position to use the spirit of Lemma 3.1 to tackle these problems. For the function g under

consideration, we have

$$\begin{aligned}
& \sup_{\theta} g\left(\left\|\sum_{i=1}^n \Phi^{L-1}(\mathbf{x}_i) \dots \mathbf{W}^2 \Phi^1(\mathbf{x}_i) \epsilon_i \mathbf{W}^1 \mathbf{b}(\mathbf{x}_i)\right\|_{\infty}\right) \\
& \leq 2 \sup_{\mathbf{W}^{L-1} \in \mathbb{R}^{m_{L-1}}} g\left(\sum_{i=1}^n \sigma'(\mathbf{W}^{L-1} \sigma(\dots \mathbf{x}_i)) \mathbf{W}^{L-1} \dots \mathbf{W}^2 \Phi^1(\mathbf{x}_i) \epsilon_i \mathbf{W}^1 \mathbf{b}(\mathbf{x}_i)\right) \\
& \stackrel{(1)}{\leq} 2 \sup_{\mathbf{W}^{L-1} \in \mathbb{R}^{m_{L-1}}} g\left(\sum_{i=1}^n \mathbf{W}^{L-1} \dots \mathbf{W}^2 \Phi^1(\mathbf{x}_i) \epsilon_i \mathbf{W}^1 \mathbf{b}(\mathbf{x}_i)\right) \\
& = 2 \sup_{\mathbf{W}^{L-1} \in \mathbb{R}^{m_{L-1}}} g\left(\mathbf{W}^{L-1} \sum_{i=1}^n \Phi^{L-1} \dots \mathbf{W}^2 \Phi^1(\mathbf{x}_i) \epsilon_i \mathbf{W}^1 \mathbf{b}(\mathbf{x}_i)\right) \\
& \stackrel{(2)}{\leq} 2 \sup g(M(L-1) \left\|\sum_{i=1}^n \Phi^{L-2} \dots \mathbf{W}^2 \Phi^1(\mathbf{x}_i) \epsilon_i \mathbf{W}^1 \mathbf{b}(\mathbf{x}_i)\right\|_{\infty})
\end{aligned} \tag{54}$$

where (1) is due to the contraction lemma of Rademacher complexity in Lemma B.2 and the fact that $|\sigma'(x)| \leq 1$. Concretely, we view then term besides the $\sigma'(\dots)$ term as a function class (for instance denote it as \mathcal{F}), and we are computing the Rademacher complexity of $\sigma'(\dots) \cdot \mathcal{F}$, which allows us to apply Lemma B.2 by noting that $|\sigma'| \leq 1$. Furthermore, (2) is due to Holder inequality.

Hence, we can apply the above discussion to the Rademacher complexity quantity and do peeling correspondingly.

$$\begin{aligned}
n\text{Rad}(\mathcal{F}_2; S) & \stackrel{(1)}{\leq} \frac{1}{\lambda} \log \mathbb{E}_{\epsilon} \sup \exp(\lambda M(L) \left\|\sum_{i=1}^n \Phi^{L-1} \dots \mathbf{W}^2 \Phi^1(\mathbf{x}_i) \epsilon_i \mathbf{W}^1 \mathbf{b}(\mathbf{x}_i)\right\|_{\infty}) \\
& \leq \frac{1}{\lambda} \log 2 \mathbb{E}_{\epsilon} \sup \exp(\lambda M(L) M(L-1) \left\|\sum_{i=1}^n \Phi^{L-2} \dots \mathbf{W}^2 \Phi^1(\mathbf{x}_i) \epsilon_i \mathbf{W}^1 \mathbf{b}(\mathbf{x}_i)\right\|_{\infty}).
\end{aligned} \tag{55}$$

where (1) is due to Jensen's inequality. So far, we have peeled the L -th and $L-1$ -th layer of the neural network outside the norm. Therefore, we can do so recursively, i.e., we can gradually peel each layer of the neural network out of the norm, which can simplify the expression a lot.

$$\begin{aligned}
n\text{Rad}(\mathcal{F}_2; S) & \leq \frac{1}{\lambda} \log 2^{L-2} \mathbb{E}_{\epsilon} \sup_{\mathbf{W}^1 \in \mathbb{R}^d} \exp\left(\lambda \prod_{l=2}^L M(l) \left|\sum_{i=1}^n \sigma'(\mathbf{W}^1 \mathbf{x}_i) \epsilon_i \mathbf{W}^1 \mathbf{b}(\mathbf{x}_i)\right|\right) \\
& \leq \frac{1}{\lambda} \log 2^{L-2} \mathbb{E}_{\epsilon} \sup_{\mathbf{W}^1 \in \mathbb{R}^d} \exp\left(\lambda \prod_{l=2}^L M(l) \left\|\mathbf{W}^1 \sum_{i=1}^n \sigma'(\mathbf{W}^1 \mathbf{x}_i) \epsilon_i \mathbf{b}(\mathbf{x}_i)\right\|\right) \\
& \leq \frac{1}{\lambda} \log 2^{L-2} \mathbb{E}_{\epsilon} \sup_{\mathbf{W}^1 \in \mathbb{R}^d} \exp\left(\lambda \prod_{l=1}^L M(l) \left\|\sum_{i=1}^n \sigma'(\mathbf{W}^1 \mathbf{x}_i) \epsilon_i \mathbf{b}(\mathbf{x}_i)\right\|_{\infty}\right).
\end{aligned} \tag{56}$$

After the peeling operations, we only need to focus on a much simpler function class which has the form of

$\sigma'(\mathbf{W}^1 \mathbf{x}_i) \mathbf{b}(\mathbf{x}_i)$.

$$\begin{aligned}
n\text{Rad}(\mathcal{F}_2; S) &\leq \frac{1}{\lambda} \log 2^{L-2} \mathbb{E}_\epsilon \sup_{\mathbf{W}^1 \in \mathbb{R}^d} \sup_{\alpha} \exp(\lambda \prod_{l=1}^L M(l) \left| \sum_{i=1}^n \sigma'(\mathbf{W}^1 \mathbf{x}_i) \epsilon_i \mathbf{b}_\alpha(\mathbf{x}_i) \right|) \\
&\leq \frac{1}{\lambda} \log 2^{L-1} \mathbb{E}_\epsilon \sup_{\mathbf{W}^1 \in \mathbb{R}^d} \sup_{\alpha} \exp(\lambda \prod_{l=1}^L M(l) \sum_{i=1}^n \sigma'(\mathbf{W}^1 \mathbf{x}_i) \epsilon_i \mathbf{b}_\alpha(\mathbf{x}_i)) \\
&\stackrel{(2)}{\leq} \frac{1}{\lambda} \log 2^{L-1} \mathbb{E}_\epsilon \sup_{\mathbf{W}^1 \in \mathbb{R}^d} \sup_{\alpha} \exp(\lambda K \prod_{l=1}^L M(l) \sum_{i=1}^n \sigma'(\mathbf{W}^1 \mathbf{x}_i) \epsilon_i) \\
&\stackrel{(3)}{\leq} \frac{1}{\lambda} \log 2^{L-1} \mathbb{E}_\epsilon \sup_{\mathbf{W}^1 \in \mathbb{R}^d} \sup_{\alpha} \exp(\lambda K \prod_{l=1}^L M(l) \sum_{i=1}^n \mathbf{W}^1 \mathbf{x}_i \epsilon_i) \\
&\leq \frac{1}{\lambda} \log 2^L \mathbb{E}_\epsilon \exp(\lambda K M(1) \prod_{l=1}^L M(l) \left\| \sum_{i=1}^n \mathbf{x}_i \epsilon_i \right\|_\infty) \\
&\stackrel{(4)}{\leq} 2KM(1) \prod_{l=1}^L M(l) \sqrt{(L+1 + \log(d))n}
\end{aligned} \tag{57}$$

where in (2) we view the $\sigma'(\mathbf{W}^1 \mathbf{x}_i)$ as the function class whose Rademacher complexity to be computed (denoted as \mathcal{F}). We are actually dealing with $\mathbf{b}_\alpha(\mathbf{x}) \mathcal{F}$, which allows us to apply the contraction lemma Lemma B.2. In (3) we use the fact that σ' is 1-Lipschitz. In (4) we use the intermediate result during proving Lemma 3.1, with $\prod_{l=1}^L M(l)$ in Lemma 3.1 replaced by $KM(1) \prod_{l=1}^L M(l)$ in this lemma.

So we get the Rademacher complexity of \mathcal{F}_2

$$\text{Rad}(\mathcal{F}_2; S) \leq 2KM(1) \prod_{l=1}^L M(l) \sqrt{\frac{L+1 + \log(d)}{n}}. \tag{58}$$

Lastly we consider the function class \mathcal{F}_1 . Recall that

$$\frac{\partial^2 u_\theta(\mathbf{x})}{\partial \mathbf{x}^2} = \left\{ \sum_{l=1}^{L-1} (\mathbf{W}^L \Phi^{L-1} \dots \mathbf{W}^{l+1}) \text{diag}(\Psi^l \dots \Psi^1 \mathbf{W}_{:,j}^1) (\mathbf{W}^l \dots \Phi^1 \mathbf{W}^1) \right\}_{1 \leq j \leq d}, \tag{59}$$

where

$$\Psi^l = \text{diag}[\sigma''(\mathbf{W}^l \sigma(\mathbf{W}^{l-1} \sigma(\dots \sigma(\mathbf{W}^1 \mathbf{x}))))]. \tag{60}$$

There are $d(L-1)$ terms due to the sum from 1 to $L-1$ and d vectors in the second order derivatives. We consider one of the $d(L-1)$ terms

$$\mathbf{W}^L \Phi^{L-1} \dots \mathbf{W}^{l+1} \text{diag}(\Psi^l \dots \Psi^1 \mathbf{W}_{:,j}^1) \mathbf{W}^l \dots \Phi^1 \mathbf{W}^1 \mathbf{A}_{:,j} : \mathbb{R}^d \rightarrow \mathbb{R}. \tag{61}$$

The only difference in dealing with \mathcal{F}_1 compared to \mathcal{F}_2 is the matrix $\text{diag}(\Psi^l \dots \Psi^1 \mathbf{W}_{:,j}^1)$ term. We first note that $|\text{diag}(\Psi^l \dots \Psi^1 \mathbf{W}_{:,j}^1)| \leq M(1)I$. The difficulty lies in the fact that for the matrix $\text{diag}(\Psi^l \dots \Psi^1 \mathbf{W}_{:,j}^1)$ to achieve the supreme, we should consider parameters at all of the 1-st to l -th layers, while in the case of \mathcal{F}_2 , the corresponding matrix Φ^l at the same position only require us to consider \mathbf{W}^L and then we successfully transform this into vector. Fortunately, we can view the parameters in the matrix $\text{diag}(\Psi^l \dots \Psi^1 \mathbf{W}_{:,j}^1)$ as a copied version of the original

parameters, i.e. U^l to circumvent the obstacle. Concretely, we have

$$\begin{aligned}
& \mathbb{E}_\epsilon \sup_{\mathbf{W}'_1} \left\| \sum_{i=1}^n \text{diag}(\Psi^l \dots \Psi^1 \mathbf{W}'_{:,j}) \mathbf{W}^l \dots \Phi^1 \mathbf{W}^1 \mathbf{A}_{:,j} \epsilon_i \right\|_\infty \\
& \leq \mathbb{E}_\epsilon \sup_{\mathbf{W}'_1, \mathbf{U}'_1} \left\| \sum_{i=1}^n \text{diag}(\Psi^l \dots \Psi^1 \mathbf{U}'_{:,j}) \mathbf{W}^l \dots \Phi^1 \mathbf{W}^1 \mathbf{A}_{:,j} \epsilon_i \right\|_\infty \\
& \leq \mathbb{E}_\epsilon \sup_{\mathbf{W}'_1, \mathbf{U}'_1} \left\| \sum_{i=1}^n \text{diag}(\sigma'(U^l \dots) \dots \sigma'(U^1 \mathbf{x}) \mathbf{U}'_{:,j}) \mathbf{W}^l \dots \Phi^1 \mathbf{W}^1 \mathbf{A}_{:,j} \epsilon_i \right\|_\infty \\
& \leq \mathbb{E}_\epsilon \sup_{\mathbf{W}^l \in \mathbb{R}^{m^{l-1}}, \mathbf{U}'_1} \left\| \sum_{i=1}^n \text{diag}(\sigma'(U^l \dots) \dots \sigma'(U^1 \mathbf{x}) \mathbf{U}'_{:,j}) \mathbf{W}^l \dots \Phi^1 \mathbf{W}^1 \mathbf{A}_{:,j} \epsilon_i \right\|_\infty \tag{62} \\
& = \mathbb{E}_\epsilon \sup_{\mathbf{W}^l \in \mathbb{R}^{m^{l-1}}, \mathbf{U}'_1} \left| \sum_{i=1}^n \text{diag}(\sigma'(U^l \dots) \dots \sigma'(U^1 \mathbf{x}) \mathbf{U}'_{:,j}) \mathbf{W}^l \dots \Phi^1 \mathbf{W}^1 \mathbf{A}_{:,j} \epsilon_i \right| \\
& \leq 2 \mathbb{E}_\epsilon \sup_{\mathbf{W}^l \in \mathbb{R}^{m^{l-1}}, \mathbf{U}'_1} \sum_{i=1}^n \text{diag}(\sigma'(U^l \dots) \dots \sigma'(U^1 \mathbf{x}) \mathbf{U}'_{:,j}) \mathbf{W}^l \dots \Phi^1 \mathbf{W}^1 \mathbf{A}_{:,j} \epsilon_i \\
& \leq 2M(1) \mathbb{E}_\epsilon \sup_{\mathbf{W}^l \in \mathbb{R}^{m^{l-1}}} \sum_{i=1}^n \mathbf{W}^l \dots \Phi^1 \mathbf{W}^1 \mathbf{A}_{:,j} \epsilon_i. \\
& \text{Rad}(\mathcal{F}_1; S) \leq 2d(L-1)KM(1)^2 \prod_{l=1}^L M(l) \sqrt{\frac{L+1+\log(d)}{n}}. \tag{63}
\end{aligned}$$

To sum up

$$\begin{aligned}
\text{Rad}(\mathcal{PINN}_M^L; S) & \leq \text{Rad}(\mathcal{F}_1; S) + \text{Rad}(\mathcal{F}_2; S) + \text{Rad}(\mathcal{F}_3; S) \\
& \leq 2K[1 + M(1) + d(L-1)M(1)^2] \prod_{l=1}^L M(l) \sqrt{\frac{L+1+\log(d)}{n}}. \tag{64}
\end{aligned}$$

□

Remark. We observe that the Rademacher complexity is composed of 3 terms, where the first is complexity of vanilla networks, the second is that of first order derivatives and the third is that of second order derivatives. Looking at the main terms, we can see that for vanilla networks, its complexity depends on $\prod_{l=1}^L M(l)$. For first order derivatives are $M(1) \prod_{l=1}^L M(l)$ and for second order derivatives are $M(1)^2 \prod_{l=1}^L M(l)$. We can see that after differentiation, the complexity is multiplied by $M(1)$, i.e. the $1, \infty$ norm of the first layer parameters. We use two-layer networks to give some intuition. Consider $u(x, \theta) = a\sigma(wx)$. The complexity of u depends on aw . $u'(x) = a\sigma'(wx)w$ and $u''(x) = a\sigma''(wx)w^2$, thus the complexity of the former depends on aww and that of the latter depends on aww^2 , which are all multiplied by the parameters at the first layer.

Discussion. To finish this subsection, we review the results and compare them to those in [23]. We have adopted the same idea as Theorem 2 in [23] in order to alleviate the dependency on depth of complexity, which gives us a tight and appropriate bound to explain generalization. Furthermore, Theorem 2 in [23] is also compatible with the Barron space theory, sine activation function for PINN, and the expressions of differentiated networks. Readers may doubt whether Theorem 1 which controls complexity via Frobenius norm and Theorem 5 which totally eliminates the dependency on depth can be applied to PINNs. Although Theorem 5 in [23] is a tighter bound, its expression is too complicated to be numerically validated. Unfortunately, Theorem 1 in [23] does not work for the sine activation used for PINNs. We can even provide counterexample where complexity cannot be controlled, based on the property of sine activation.

C Proofs of Main Results

C.1 Proof of Theorem 3.1

Proof. (Proof of Theorem 3.1) Let \hat{u}_m parameterized by $\hat{\theta}$ be like in Theorem 2.3, i.e.

$$\begin{aligned}
\|\hat{u}_m - u^*\|_{L^2(\mathbb{P})} & \leq \frac{3L\|u^*\|_{\mathcal{W}^L}}{\sqrt{m}}, \\
\|\hat{\theta}\|_{\mathcal{P}} & \leq \|u^*\|_{\mathcal{W}^L(\Omega)}. \tag{65}
\end{aligned}$$

where take the probability measure \mathbb{P} as

$$\mathbb{P} = \frac{n_r}{n} \text{Unif}(\Omega) + \frac{1}{n} \sum_{\mathbf{x} \in S \cap \partial\Omega} \delta_{\mathbf{x}}, \quad (66)$$

which means \mathbb{P} contains empirical distribution of boundary training points and the uniform distribution within Ω for using Assumption 3.2. Thus, by Assumption 3.2, we have

$$\mathbb{E}_{\mathbf{x} \in S \cap \Omega} (\mathcal{L}\hat{u}_m(\mathbf{x}) - \mathcal{L}u^*(\mathbf{x}))^2 = \frac{1}{n_r} \sum_{i=1}^{n_r} (\mathcal{L}\hat{u}_m(\mathbf{x}_{r,i}) - \mathcal{L}u^*(\mathbf{x}_{r,i}))^2 \leq \frac{3C_{pde}L\|u^*\|_{\mathcal{W}^L(\Omega)}}{\sqrt{m}} \quad (67)$$

Then by definition,

$$\begin{aligned} R_S(\boldsymbol{\theta}_{S,\lambda}) + \lambda \|\boldsymbol{\theta}_{S,\lambda}\|_{\mathcal{P}}^2 &\leq R_S(\hat{\boldsymbol{\theta}}) + \lambda \|\hat{\boldsymbol{\theta}}\|_{\mathcal{P}}^2 \\ &\leq \frac{9C_{pde}^2 L^2 \|u^*\|_{\mathcal{W}^L(\Omega)}^2}{m} + \lambda \|u^*\|_{\mathcal{W}^L(\Omega)}^2. \end{aligned} \quad (68)$$

In particular,

$$\|u_m\|_{\mathcal{W}^L} \leq \|\boldsymbol{\theta}\|_{\mathcal{P}} \leq \frac{2\lambda \|u^*\|_{\mathcal{W}^L(\Omega)}}{\lambda} = 2\|u^*\|_{\mathcal{W}^L(\Omega)}. \quad (69)$$

The Rademacher complexity of hypothesis used for the boundary points is

$$2\sqrt{2}\|u^*\|_{\mathcal{W}^L(\Omega)} \sqrt{\frac{L+1+\log(d)}{n_b}}. \quad (70)$$

Hence,

$$R_{\mathcal{D} \cap \partial\Omega} \leq R_{S \cap \partial\Omega} + 4\sqrt{2}\|u^*\|_{\mathcal{W}^L(\Omega)} \sqrt{\frac{L+1+\log(d)}{n_b}} + c\sqrt{\frac{2\log(2/\delta)}{n_b}}. \quad (71)$$

Similarly, Rademacher complexity of the hypothesis used for residual points, i.e. the differentiated networks are $2\sqrt{2}Kd(L+1)\|u^*\|_{\mathcal{W}^L(\Omega)} \sqrt{\frac{L+1+\log(d)}{n_r}}$, thus:

$$R_{\mathcal{D} \cap \Omega} \leq R_{S \cap \Omega} + 4\sqrt{2}Kd(L+1)\|u^*\|_{\mathcal{W}^L(\Omega)} \sqrt{\frac{L+1+\log(d)}{n_r}} + c\sqrt{\frac{2\log(2/\delta)}{n_r}}. \quad (72)$$

In sum, we obtain the two generalization bounds on the boundary and in the residual respectively. \square

C.2 Proof of Theorem 3.2

Proof. (Proof of Theorem 3.2). Consider the function class

$$\mathcal{H}_Q = \left\{ l(u(\mathbf{x}), u(\mathbf{x}, \boldsymbol{\theta})) \mid \max \left[\prod_{l=1}^L M(l), M(1) \prod_{l=1}^L M(l), M(1)^2 \prod_{l=1}^L M(l), M(L) \right] \leq Q \right\}. \quad (73)$$

Then the class of composition of all neural networks and the loss function is $\mathcal{H} = \cup_{Q=1}^{\infty} \mathcal{H}_Q$. Note that

$$\begin{aligned} \sup_{\mathbf{x} \in \Omega} |u(\mathbf{x}, \boldsymbol{\theta})| &= \sup_{\mathbf{x} \in \Omega} |\mathbf{W}^L \sigma(\mathbf{W}^{L-1} \sigma(\dots \sigma(\mathbf{W}^1 \mathbf{x})))| \\ &\leq M(L) \sup_{\mathbf{x} \in \Omega} \|\sigma(\mathbf{W}^{L-1} \sigma(\dots \sigma(\mathbf{W}^1 \mathbf{x})))\|_{\infty} \\ &\leq M(L) \\ &\leq Q, \end{aligned} \quad (74)$$

where we used the fact that $|\sigma(\mathbf{x})| \leq 1$. Therefore, for functions in \mathcal{H}_Q , since we assume the target function u to be learned satisfies $u(\mathbf{x}) \leq 1$, hence we have

$$\begin{aligned} 0 \leq l(u(\mathbf{x}), u(\mathbf{x}, \boldsymbol{\theta})) &\leq \frac{1}{2}(1 + u(\mathbf{x}, \boldsymbol{\theta}))^2 \\ &\leq \frac{1}{2}(1 + M(L))^2 \\ &\leq 2Q^2, \end{aligned} \quad (75)$$

for all $\mathbf{x} \in \Omega$ and all $Q \geq 1$. We note that $l(y, \cdot)$ is a Lipschitz function with a Lipschitz constant which is no larger than $\sup_{\mathbf{x} \in \Omega} |u(\mathbf{x}, \boldsymbol{\theta})| \leq M(L) \leq Q$. Hence

$$\text{Rad}(\mathcal{H}_Q; S) \leq M(L)\text{Rad}(\mathcal{F}_Q) \leq Q\text{Rad}(\mathcal{F}_Q). \quad (76)$$

By the result of Rademacher complexity of neural networks in Lemmas 3.1 and 3.2, for any given δ and any positive integer Q with probability at least $1 - \delta_Q$ over S with $\delta_Q = \frac{6\delta}{\pi^2 Q^2}$, we have

$$\begin{aligned} \sup_{\boldsymbol{\theta}} |R_{D \cap \partial\Omega}(\boldsymbol{\theta}) - R_{S \cap \partial\Omega}(\boldsymbol{\theta})| &\leq 2Q\text{Rad}(\mathcal{F}_Q; S) + 2Q^2 \sqrt{\frac{\log(2/\delta_Q)}{2n}} \\ &\leq 4Q^2 \sqrt{\frac{L+1+\log(d)}{n}} + 2Q^2 \sqrt{\frac{\log(\pi^2 Q^2/3\delta)}{2n}}. \end{aligned} \quad (77)$$

For any parameter $\boldsymbol{\theta}$ minimizes the empirical loss, choose the integer Q such that

$$Q - 1 \leq \max\left[\prod_{l=1}^L M(l), M(1) \prod_{l=1}^L M(l), M(1)^2 \prod_{l=1}^L M(l), M(L)\right] \leq Q. \quad (78)$$

Then we have

$$\begin{aligned} |R_{D \cap \partial\Omega}(\boldsymbol{\theta}) - R_{S \cap \partial\Omega}(\boldsymbol{\theta})| &\leq 4Q^2 \sqrt{\frac{L+1+\log(d)}{n}} + Q \sqrt{\frac{\log(\pi^2 Q^2/3\delta)}{2n}} \\ &\leq 4(N+1)^2 \sqrt{\frac{L+1+\log(d)}{n}} + 2(N+1)^2 \sqrt{\frac{\log(\pi^2 (N+1)^2/3\delta)}{2n}}. \end{aligned} \quad (79)$$

where

$$N = \max\left[\prod_{l=1}^L M(l), M(1) \prod_{l=1}^L M(l), M(1)^2 \prod_{l=1}^L M(l), M(L)\right]. \quad (80)$$

The above bound just holds with probability $1 - \delta_Q$ for any pair $(\boldsymbol{\theta}, Q)$ as long as $\boldsymbol{\theta}$ satisfies $N \leq Q$. Since $\sum_{Q=1}^{\infty} \delta_Q = \delta$, the bound holds with probability $1 - \delta$.

We have already proved the generalization bound of the boundary loss in PINN. That for residual loss is similar by using the boundedness of our activation function. Specifically, let $\mathcal{G}_Q = \{l(f(\mathbf{x}), \mathcal{L}u(\mathbf{x}, \boldsymbol{\theta}) | N \leq Q)\}$. Then the class of all differentiated neural networks $\mathcal{G} = \cup_{Q=1}^{\infty} \mathcal{G}_Q$. Note that

$$\begin{aligned} \sup_{\mathbf{x} \in \Omega} |\mathcal{L}u(\mathbf{x}, \boldsymbol{\theta})| &\leq KM(L) + K \prod_{l=1}^L M(l) + d(L-1)KM(1) \prod_{l=1}^L M(l) \\ &\leq KQ + KQ + d(L-1)KQ \\ &\leq d(L+1)KQ. \end{aligned} \quad (81)$$

Therefore, for functions in \mathcal{F}_Q , since we assume $f(\mathbf{x}) \leq 1$, we have

$$\begin{aligned} 0 \leq l(f(\mathbf{x}), \mathcal{L}u(\mathbf{x}, \boldsymbol{\theta})) &\leq \frac{1}{2}(1 + \mathcal{L}u(\mathbf{x}, \boldsymbol{\theta}))^2 \\ &\leq \frac{1}{2}(1 + Kd(L+1)N)^2 \\ &\leq 2K^2 d^2 (L+1)^2 Q^2, \end{aligned} \quad (82)$$

for all $\mathbf{x} \in \Omega$ and all $Q \geq 1$. We note that $l(y, \cdot)$ is a Lipschitz function with a Lipschitz constant which is no larger than $\sup_{\mathbf{x} \in \Omega} |\mathcal{L}u(\mathbf{x}, \boldsymbol{\theta})| \leq Kd(L+1)N$. Hence

$$\text{Rad}(\mathcal{G}_Q; S) \leq K(L+1)N\text{Rad}(\mathcal{F}_Q) \leq K(L+1)Q\text{Rad}(\mathcal{F}_Q). \quad (83)$$

By the result of Rademacher complexity of neural networks in Lemma 3.2, for any given δ and any positive integer Q

with probability at least $1 - \delta_Q$ over S with $\delta_Q = \frac{6\delta}{\pi^2 Q^2}$, we have

$$\begin{aligned}
& \sup_{\boldsymbol{\theta}: N \leq Q} |R_{D \cap \Omega}(\boldsymbol{\theta}) - R_{S \cap \Omega}(\boldsymbol{\theta})| \\
& \leq 2Kd(L+1)Q \text{Rad}(\mathcal{F}_Q; S) + 2K^2 d^2 (L+1)^2 Q^2 \sqrt{\frac{\log(2/\delta_Q)}{2n}} \\
& \leq 2Kd(L+1)Q \cdot 2K[1 + M(1) + d(L-1)M(1)^2] \prod_{l=1}^L M(l) \sqrt{\frac{L+1 + \log(d)}{n}} + \\
& \quad 2K^2 d^2 (L+1)^2 Q^2 \sqrt{\frac{\log(\pi^2 Q^2 / 3\delta)}{2n}} \\
& \leq 2Kd(L+1)Q \cdot 2K[Q + Q + d(L-1)Q] \sqrt{\frac{L+1 + \log(d)}{n}} + \\
& \quad 2K^2 d^2 (L+1)^2 Q^2 \sqrt{\frac{\log(\pi^2 Q^2 / 3\delta)}{2n}} \\
& \leq 4K^2 d^2 (L+1)^2 Q^2 \sqrt{\frac{L+1 + \log(d)}{n}} + 2K^2 d^2 (L+1)^2 Q^2 \sqrt{\frac{\log(\pi^2 Q^2 / 3\delta)}{2n}}.
\end{aligned} \tag{84}$$

For any parameter $\boldsymbol{\theta}$ minimizes the empirical loss, choose the integer Q such that $Q - 1 \leq N \leq Q$ for it. Then we have

$$\begin{aligned}
& |R_{D \cap \Omega}(\boldsymbol{\theta}) - R_{S \cap \Omega}(\boldsymbol{\theta})| \\
& \leq 4K^2 d^2 (L+1)^2 Q^2 \sqrt{\frac{L+1 + \log(d)}{n}} + 2K^2 d^2 (L+1)^2 Q^2 \sqrt{\frac{\log(\pi^2 Q^2 / 3\delta)}{2n}} \\
& \leq 4K^2 d^2 (L+1)^2 (N+1)^2 \sqrt{\frac{L+1 + \log(d)}{n}} + \\
& \quad 2K^2 d^2 (L+1)^2 (N+1)^2 \sqrt{\frac{\log(\pi^2 (N+1)^2 / 3\delta)}{2n}}.
\end{aligned} \tag{85}$$

The above bound just holds with probability $1 - \delta_Q$ for any pair $(\boldsymbol{\theta}, Q)$ as long as $\boldsymbol{\theta}$ satisfies $Q - 1 \leq N \leq Q$. Since $\sum_{Q=1}^{\infty} \delta_Q = \delta$, the bound holds with probability $1 - \delta$. \square

D Related Work

In this section, we summarize related works. We focus on related works on PINNs, Rademacher complexity of neural networks, and the theory of PINNs.

D.1 Physics-Informed Neural Networks

We first introduce some background on physics-informed neural networks (PINNs), which are the models we have considered throughout this paper.

Due to its success in approximating high-dimensional functions while generalizing well, deep learning has been used to solve partial differential equations (PDEs). Among them, PINNs [6] approximate the solutions of PDEs by neural networks, and then optimize them by stochastic gradient descent for expectation minimization to let them satisfy the physical rule described by the PDE. Later, the extended PINNs (XPINNs) [12] which adopt domain decomposition methods show faster convergence and better generalization performances than vanilla PINNs, but the underlying reason for this remains unknown. Prior to XPINN, CPINN [25] is also a domain decomposition-based PDE solver. However, CPINN is only applicable to conservation laws and does not allow the general spatio-temporal domain decomposition.

To the best of our knowledge, the present work provides the first proof on generalization of PINNs and XPINNs, and the first analysis on when and how XPINNs perform better than PINNs.

D.2 Rademacher Complexity of Neural Networks

In this subsection, we review the Rademacher complexity of neural networks, which plays a key role in our generalization theory on PINNs and XPINNs.

In statistical learning theory, the Rademacher complexity measures the richness of a class of functions on which the generalization error bound is based. In the literature, there have been various controls and estimations on the Rademacher complexity of the class of neural network functions.

There are various ways to bound the Rademacher complexity of the class of neural networks, namely the norm-based control (adopted in this study), and sharpness. For norm-based capacity control, [26] bounds Rademacher complexity by product of Frobenius norms of parameter matrices. However, their bounds grow exponentially as the depth increases, which contradicts the fact that deeper networks generalize better. To eliminate the exponential dependency on network

depth, [24] uses a covering number approach to show a bound scaling as $O(\frac{\prod_{l=1}^L \|\mathbf{W}^l\| (\sum_{l=1}^L (\frac{\|\mathbf{W}^{lT}\|_{2,1}}{\|\mathbf{W}^l\|})^{\frac{2}{3}})^{\frac{2}{3}}}{\sqrt{m}})$. Although the explicit dependency on network depth L disappears, the bound still has polynomial dependency (L^3) on the depth due to the fact that $\|\mathbf{W}^{lT}\|_{2,1} \geq \|\mathbf{W}^l\|$. To derive size-independent sample complexity for neural networks, [23] further proves several useful results. Firstly, [23] improves the dependency on depth from L^3 in [24] to \sqrt{L} . Secondly, [23] uses Shatten p -norms of matrices to derive bounds which totally remove any dependency on the depth. [19] empirically validates the effectiveness of these norm-based capacity controls to explain the generalization mystery of deep learning. Another line of work focuses on sharpness, which adopts robustness of the training error to the perturbations in the parameters as a complexity measure for neural networks. [27] combines sharpness measure with PAC-Bayesian approach, providing a generalization bound scaling at $O(\frac{\prod_{l=1}^L \|\mathbf{W}^l\| (\sum_{l=1}^L (\frac{\|\mathbf{W}^l\|_F}{\|\mathbf{W}^l\|})^{\frac{2}{3}})^{\frac{2}{3}}}{\sqrt{m}})$, which is shown to be similar to the bound in [24] when weights are sparse, and tighter than [24] when the weights are fairly dense and are of uniform magnitude.

In this paper, we mainly consider Theorem 2 in [23] to control the Rademacher complexity of PINNs. We discuss why other kinds of complexity controls cannot be applied to PINNs in the Appendix.

D.3 Theory on PINNs

Due to the success of PINNs in approximating high-dimensional complicated functions such as solutions of PDEs, theoretical evidence accounting for the outstanding empirical performance has increasingly attracted considerable attention.

The most related work is [13], where the authors consider Barron space for two-layer networks for prior and posterior generalization bounds. [13] also leverages neural tangent kernel to show global convergence of PINNs. [15] introduces an abstract formalism and the stability properties of the underlying PDE are leveraged to derive an estimate for the generalization error in terms of the training error and number of training samples. By adapting the Schauder approach and the maximum principle, [16] shows that as number of training samples go to infinity, the minimizer converges to the solution in C^0 and H^1 . [14] uses the Barron space for two-layer neural networks to provide a prior analysis on PINN with softplus activation, via adopting the similarity between softplus and ReLU.

Our work extends existing results to multi-layer networks, which is more general and realistic, and considers various kinds of capacity controls for PINNs, namely the Barron norm and the $1, \infty$ norm. Extensive experiments and analytical examples further validate the effectiveness of our theory. Our work is also the first to analyze when and how XPINN is better than PINN.

E Discussion

E.1 Why Barron Space?

This subsection is devoted to clarify why we choose Barron space theory for developing our prior bound. Overall, it has the following two advantages.

Firstly, we should choose a theory that can measure complexity of both networks and target functions, which plays a key role in the prior generalization bound in Theorem 3.1. In the Barron space, we are able to measure the complexity of target functions easily via Barron norm, and we can further show that complexities of trained neural networks are controlled by that of the target functions. Since the success of deep learning owns to its data-dependent training, i.e. although the class of networks has huge complexity, gradient descent does find out a simple network, which is reflected by the Barron space theory.

Secondly, the Barron space in high dimension neural networks resembles Sobolev and Besov space which are indispensable building blocks for low dimension classical theory. A proper function space is essential in analyzing PDEs. The class of network functions define a natural function space, i.e. the Barron space. By studying the target function of the PDE problem in the Barron space by its norm, the generalization error of the trained network can be obtained in terms of that norm. This reasoning resembles prior error analysis in classical finite element method where the error is controlled by the Sobolev norm of the target. Therefore, the Barron space adopted is appropriate for PDE analysis.

E.2 Different Rademacher Complexity Control for PINNs

Untill now, we have used the products of the $1, \infty$ norm $\|\mathbf{W}^l\|_{1, \infty}$ of the parameters matrices at each layer to bound the Rademacher complexity of neural networks, which is originally derived in Theorem 2 of [23]. Our contribution is to extend it to PINNs.

One may doubt that Theorem 2 of [23] is not the best result for complexity of networks, actually in [23] the authors prove better results that even get rid of the exponential dependence on the depth. Why don't we choose the better results in this paper? There are mainly two reasons.

The first reason is that this result is good enough, since it improves the exponential dependence of complexity on network depth to a polynomial one. The second reason is that other state-of-the-art Rademacher complexity measures are unfortunately incompatible with the expression of PINNs. In the following, we briefly summarize other available complexity measures and introduce their incompatibility.

In the literature, there are mainly norm-based capacity control and sharpness based complexity control. For the norm based control, the better bound in Theorem 5 of [23] uses the Schatten norm. Even though it eliminates all dependency on network depth, its expression is too complicated to be numerically computed. Moreover, the technique proving the result cannot be applied to differentiated networks, meaning that the bound doesn't apply to PINNs. The bound based on Frobenius norm in Theorem 1 of [23] does not hold for PINNs activated by smooth activation like sine and tanh. The bound based on spectral norm in [24] still cannot be applied to PINNs, which implicitly has an polynomial dependency on the depth. Under the spectral norm case for Rademacher complexity, we cannot perform the "peeling" technique as what have done in the case of $1, \infty$ norm. The sharpness based approaches cannot be applied to PINNs because the change of PINNs after perturbation is harder to control due to the differentiation.

In sum, we have shown in this subsection that the approach adopting $1, \infty$ matrix norm for capacity control is both tight and applicable to PINNs.

F Additional Comparison

F.1 Comparison of Boundary Loss via Theorem 3.1

The comparison will be done via computing their respective theoretical bounds. In particular, the generalization performance of PINN depends on the upper bound in Theorem 3.1, which is

$$R_{S \cap \partial \Omega} + 4\sqrt{2}\|u^*\|_{\mathcal{W}^L(\Omega)} \sqrt{\frac{L+1+\log(d)}{n_b}} + c\sqrt{\frac{2\log(2/\delta)}{n_b}}, \quad (86)$$

where n_b is the number of boundary training points.

For XPINN's generalization, we can apply Theorem 3.1 to each of the subdomains in XPINN. Specifically, for the i -th sub-net in the i -th subdomain, i.e. the $\Omega_i, i \in \{1, 2, \dots, N_D\}$, its generalization performance is upper bounded by

$$R_{S \cap \partial \Omega_i} + 4\sqrt{2}\|u^*\|_{\mathcal{W}^L(\Omega_i)} \sqrt{\frac{L+1+\log(d)}{n_{b,i}}} + c\sqrt{\frac{2\log(2/\delta)}{n_{b,i}}}, \quad (87)$$

where $n_{b,i}$ is the number of training boundary points in the i -th subdomain.

Hence, since the i -th subdomain has $n_{b,i}$ training boundary points and is in charge of the prediction of $\frac{n_{b,i}}{n_b}$ proportion of testing data, we weighted average their generalization errors to get the generalization error of XPINN

$$\sum_{i=1}^{N_D} \frac{n_{b,i}}{n_b} (R_{S \cap \partial \Omega_i} + 4\sqrt{2}\|u^*\|_{\mathcal{W}^L(\Omega_i)} \sqrt{\frac{L+1+\log(d)}{n_{b,i}}} + c\sqrt{\frac{2\log(2/\delta)}{n_{b,i}}}), \quad (88)$$

If we omit the last term and assume the empirical losses of PINN and XPINN are similar, i.e.

$$R_{S \cap \partial \Omega} \approx \sum_{i=1}^{N_D} \frac{n_{b,i}}{n_b} R_{S \cap \partial \Omega_i}, c\sqrt{\frac{2\log(2/\delta)}{n_{b,i}}} \ll \|u^*\|_{\mathcal{W}^L(\Omega)}, \|u^*\|_{\mathcal{W}^L(\Omega_i)}, \quad (89)$$

then comparing the generalization ability of PINN and XPINN reduces to the following comparison:

$$\underbrace{\|u^*\|_{\mathcal{W}^L(\Omega)}}_{\text{PINN}} \quad \text{versus} \quad \underbrace{\sum_{i=1}^{N_D} \sqrt{\frac{n_{b,i}}{n_b}} \|u^*\|_{\mathcal{W}^L(\Omega_i)}}_{\text{XPINN}}, \quad (90)$$

where model having smaller corresponding quantity is more generalizable.

F.2 Comparison of Boundary Loss via Theorem 3.2

In this subsection, we compare PINN with XPINN by Theorem 3.2, where we focus on the boundary losses of PINN and XPINN. we denote the upper bound of PINN testing loss as B_{PINN} and those of the sub-net i in XPINN as $B_{i,\text{XPINN}}$, $i \in \{1, 2, \dots, N_D\}$ which are provided by the right sides of Theorem 3.2, i.e. the bounds are

$$\begin{aligned} B_{\text{PINN}} &= 2(N+1)^2 \left(2\sqrt{\frac{L+1+\log(d)}{n_b}} + \sqrt{\frac{\log(\pi^2(N+1)^2/3\delta)}{2n_b}} \right), \\ B_{i,\text{XPINN}} &= 2(N_i+1)^2 \left(2\sqrt{\frac{L+1+\log(d)}{n_{b,i}}} + \sqrt{\frac{\log(\pi^2(N_i+1)^2/3\delta)}{2n_{b,i}}} \right), \end{aligned} \quad (91)$$

where \mathbf{W}^l is the l -th layer weight matrix of the PINN model, $M(l) = \|\mathbf{W}^l\|_{1,\infty}$ and N defined in Theorem 3.2. Besides, \mathbf{W}_i^l is the l -th layer weight matrix of the i -th sub-net in the XPINN model, $M_i(l) = \|\mathbf{W}_i^l\|_{1,\infty}$ and

$$N_i = \max\left[\prod_{l=1}^L M_i(l), M_i(1) \prod_{l=1}^L M_i(l), M_i(1)^2 \prod_{l=1}^L M_i(l), M_i(L)\right], \quad (92)$$

is the N quantity for the i -th sub-net. Since the i -th sub-net in XPINN is in charge of the prediction of $\frac{n_{b,i}}{n_b}$ proportion of testing data, we weighted average their generalization errors to get that of XPINN, i.e. $B_{\text{XPINN}} = \sum_{i=1}^{N_D} \frac{n_{b,i}}{n_b} B_{i,\text{XPINN}}$ where B_{XPINN} is the bound for XPINN. Thus, we are only required to compare B_{PINN} with B_{XPINN} , where model having smaller corresponding quantity is more generalizable.

References

- [1] Ameya D Jagtap, Kenji Kawaguchi, and George Em Karniadakis. Adaptive activation functions accelerate convergence in deep and physics-informed neural networks. *Journal of Computational Physics*, 404:109136, 2020.
- [2] Kenji Kawaguchi. Deep learning without poor local minima. In *Advances in neural information processing systems (NeurIPS)*, pages 586–594, 2016.
- [3] Keyulu Xu, Mozhi Zhang, Stefanie Jegelka, and Kenji Kawaguchi. Optimization of graph neural networks: Implicit acceleration by skip connections and more depth. In *International Conference on Machine Learning (ICML)*, 2021.
- [4] Kenji Kawaguchi. On the theory of implicit deep learning: Global convergence with implicit layers. In *International Conference on Learning Representations (ICLR)*, 2021.
- [5] Kenji Kawaguchi, Leslie Pack Kaelbling, and Yoshua Bengio. Generalization in deep learning. *In Mathematics of Deep Learning, Cambridge University Press, to appear. Preprint available as: MIT-CSAIL-TR-2018-014, Massachusetts Institute of Technology*, 2018.
- [6] Maziar Raissi, Paris Perdikaris, and George E Karniadakis. Physics-informed neural networks: A deep learning framework for solving forward and inverse problems involving nonlinear partial differential equations. *Journal of Computational Physics*, 378:686–707, 2019.
- [7] Shengze Cai, Zhicheng Wang, Sifan Wang, Paris Perdikaris, and George Em Karniadakis. Physics-Informed Neural Networks for Heat Transfer Problems. *Journal of Heat Transfer*, 143(6), 04 2021. ISSN 0022-1481. doi: 10.1115/1.4050542. URL <https://doi.org/10.1115/1.4050542>. 060801.
- [8] Minglang Yin, Xiaoning Zheng, Jay D Humphrey, and George Em Karniadakis. Non-invasive inference of thrombus material properties with physics-informed neural networks. *Computer Methods in Applied Mechanics and Engineering*, 375:113603, 2021.
- [9] Yuyao Chen, Lu Lu, George Em Karniadakis, and Luca Dal Negro. Physics-informed neural networks for inverse problems in nano-optics and metamaterials. *Optics express*, 28(8):11618–11633, 2020.
- [10] Shengze Cai, Zhicheng Wang, Frederik Fuest, Young Jin Jeon, Callum Gray, and George Em Karniadakis. Flow over an espresso cup: inferring 3-d velocity and pressure fields from tomographic background oriented schlieren via physics-informed neural networks. *Journal of Fluid Mechanics*, 915, 2021.
- [11] Xiaowei Jin, Shengze Cai, Hui Li, and George Em Karniadakis. NSFnets (Navier-Stokes flow nets): Physics-informed neural networks for the incompressible navier-stokes equations. *Journal of Computational Physics*, 426:109951, 2021.
- [12] Ameya D Jagtap and George Em Karniadakis. Extended physics-informed neural networks (xpinns): A generalized space-time domain decomposition based deep learning framework for nonlinear partial differential equations. *Communications in Computational Physics*, 28(5):2002–2041, 2020.
- [13] Tao Luo and H. Yang. Two-layer neural networks for partial differential equations: Optimization and generalization theory. *ArXiv*, abs/2006.15733, 2020.
- [14] Jianfeng Lu, Yulong Lu, and Min Wang. A priori generalization analysis of the deep Ritz method for solving high dimensional elliptic equations. *arXiv preprint arXiv:2101.01708*, 2021.
- [15] Siddhartha Mishra and Roberto Molinaro. Estimates on the generalization error of physics informed neural networks (PINNs) for approximating pdes. *arXiv:2006.16144*, 2020.
- [16] Yeonjong Shin, Jérôme Darbon, and George Em Karniadakis. On the convergence of physics informed neural networks for linear second-order elliptic and parabolic type pdes. *Communications in Computational Physics*, 28(5):2042–2074, 2020. ISSN 1991-7120.
- [17] E. Weinan and Stephan Wojtowytsch. On the banach spaces associated with multi-layer relu networks: Function representation, approximation theory and gradient descent dynamics. *ArXiv*, abs/2007.15623, 2020.
- [18] E. Weinan, Chao Ma, and L. Wu. A priori estimates of the generalization error for two-layer neural networks. *ArXiv*, abs/1810.06397, 2018.

- [19] Behnam Neyshabur, Srinadh Bhojanapalli, David McAllester, and Nathan Srebro. Exploring generalization in deep learning. *arXiv preprint arXiv:1706.08947*, 2017.
- [20] Peter L Bartlett and Shahar Mendelson. Rademacher and gaussian complexities: Risk bounds and structural results. *JMLR*, 3(Nov):463–482, 2002.
- [21] Diederik P Kingma and Jimmy Ba. Adam: A method for stochastic optimization. *arXiv preprint arXiv:1412.6980*, 2014.
- [22] A.R. Barron. Universal approximation bounds for superpositions of a sigmoidal function. *IEEE Transactions on Information Theory*, 39(3):930–945, 1993. doi: 10.1109/18.256500.
- [23] Noah Golowich, A. Rakhlin, and O. Shamir. Size-independent sample complexity of neural networks. In *COLT*, 2018.
- [24] Peter Bartlett, Dylan J Foster, and Matus Telgarsky. Spectrally-normalized margin bounds for neural networks. *arXiv preprint arXiv:1706.08498*, 2017.
- [25] Ameya D Jagtap, Ehsan Kharazmi, and George Em Karniadakis. Conservative physics-informed neural networks on discrete domains for conservation laws: Applications to forward and inverse problems. *Comput. Methods Appl. Mech. Engrg*, 365:113028, 2020.
- [26] Behnam Neyshabur, Ryota Tomioka, and Nathan Srebro. Norm-based capacity control in neural networks. In *Conference on Learning Theory*, pages 1376–1401. PMLR, 2015.
- [27] Behnam Neyshabur, Srinadh Bhojanapalli, and Nathan Srebro. A pac-bayesian approach to spectrally-normalized margin bounds for neural networks. *arXiv preprint arXiv:1707.09564*, 2017.